# Decoupling and its relation to strain partitioning in continental lithosphere: insight from the Periadriatic fault system (European Alps)

M. R. HANDY, J. BABIST, R. WAGNER, C. ROSENBERG & M. KONRAD
*Geowissenschaften, Freie Universität Berlin, D-12249 Germany*
*(e-mail: mhandy@zedat.fu-berlin.de)*

**Abstract:** The Periadriatic fault system (PFS) is an array of late orogenic faults (35–15 Ma) in the retro-wedge of the Alpine orogen that accommodated dextral transpression during oblique indentation by the southern Alpine crust. Decoupling along the leading edges of the southern Alpine indenter occurred where inherited lithological and rheological contrasts were accentuated by lateral thermal gradients during emplacement of the warm orogenic retro-wedge next to the cold indenter. In contrast, decoupling within the core and retro-wedge of the orogen occurred in a network of folds and mylonitic faults. In the Eastern Alps, this network comprises conjugate sets of upright, constrictional folds, strike–slip faults and low-angle normal faults that accommodated nearly coaxial NNE–SSW shortening and E–W extensional exhumation of the Tauern thermal dome. The dextral shear component of oblique convergence was taken up by a discrete, brittle fault parallel to the indenter surface. In the Central and Western Alps, a steep mylonitic backthrust, upright folds, and low-angle normal faults effected transpressional exhumation of the Lepontine thermal dome. Mylonitic thrusting and dextral strike–slip shearing along the steep indenter surface are transitional along strike to low-angle normal faults that accommodated extension at the western termination of the PFS. The areal distribution of poles to mylonitic foliation and stretching lineation of these networked structures is related to the local shape and orientation of the southern Alpine indenter surface, supporting the interpretation of this surface as the macroscopic shearing plane for all mylonitic segments of the PFS. We propose that mylonitic faults nucleate as viscous instabilities induced by cooling, or more often, by folding and progressive rotation of pre-existing foliations into orientations that are optimal for simple shearing parallel to the eigenvectors of flow. The mechanical anisotropy of the viscous continental crust makes it a preferred site of decoupling and weakening. Networking of folds and mylonitic fault zones allow the viscous crust to maintain strain compatibility between the stronger brittle crust and upper mantle, while transmitting plate forces through the lithosphere. Decoupling within the continental lithosphere is therefore governed by the symmetry and kinematics of strain partitioning at, and below, the brittle-to-viscous transition.

## Introduction

The structure of continental fault zones at strike–slip or oblique-slip plate boundaries varies with depth, from discrete faults and folds in the uppermost 5 km (e.g. Sylvester 1988), through anastomozing mylonitic shear zones in the intermediate to lower crust (Sibson 1977) to large zones of ductile, mylonitic shear in the upper mantle (Teyssier & Tikoff 1998 and references therein). This vertical change in structural style is associated with a change in kinematics: whereas displacement near the surface is partitioned into dip– and strike–slip zones that bound crustal blocks, in the lithospheric mantle it is apparently accommodated simply within a broad shear zone (Vauchez & Tommasi 2003). This necessitates a zone of accommodation somewhere in between, usually taken to be the middle to lower crust. Recent debate has centered on the nature and mechanisms of this accommodation (e.g. Tikoff *et al.* 2002).

On the one hand, intracrustal accommodation appears to involve decoupling within subhorizontal detachment layers, a view supported by the geometry of fault systems imaged in reflection seismic profiles across orogens (e.g. Schmid & Kissling 2000) and extended continental lithosphere (e.g. Davis & Lister 1988; Boillot *et al.* 1995). These show that faults root at 10–15 km depth within the crust, as well as at, or just above, the MOHO. The depths for

*From*: GAPAIS, D., BRUN, J. P. & COBBOLD, P. R. (eds) 2005. *Deformation Mechanisms, Rheology and Tectonics: from Minerals to the Lithosphere*. Geological Society, London, Special Publications, **243**, 249–276.
0305-8719/05/$15.00 

these inferred decoupling zones are corroborated by strength–depth profiles constructed from experimental flow laws for quartz-rich crustal rocks and olivine-rich mantle rocks (e.g. Brace & Kohlstedt 1980; Ranalli & Murphy 1987). On the other hand, intracrustal strain accommodation must also involve vertical coupling in order to explain coincident displacement fields for the upper crust and upper mantle, as inferred from geodetic and teleseismic observations in tectonically active areas (e.g. Holt 2000). Thus, one is left with the paradox that both strain discontinuity (detachment) and continuity (attachment) are required, within the crust and across the crust–mantle boundary.

Molnar (1992) argued, partly by reference to the analogue experiments of Richard & Cobbold (1989), that subhorizontal viscous layer(s) at the base of the brittle upper crust maintain vertical strain continuity while facilitating strain partitioning on brittle faults above. They do this because isotropic, viscous media apparently do not transmit shear stresses from below, causing the principal stress axes to be nearly orthogonal to the horizontal base of the overlying crustal blocks. Strain continuum models of Fossen & Tikoff (1998) and Teyssier *et al.* (2002) predict that intracrustal accommodation occurs within zones of continuous, three-dimensional strain just beneath the brittle crust. In contrast to strain continuum models, rheological models incorporating time-dependent brittle behaviour of the upper crust (Tse & Rice 1986; Li & Rice 1987) predict that, while viscous creep and intracrustal attachment prevail at depths below about 15 km, vertical attachment above this level is punctuated by episodic, coseismic detachment. All of these models shed valuable light on some, but not all, aspects of strain accommodation at rheological transitions in the lithosphere. The vexing question remains whether and/or to what extent strain compatibility in the lithosphere is maintained by continuous three-dimensional flow, by episodic detachment, or by some combination of both.

Resolving this debate is obviously difficult given our inability to observe the deep levels of active fault zones. Geophysical methods, although helpful in imaging some structural properties '*in situ*' (e.g. Mooney & Ginzburg 1986), provide little information on the evolution of structures and kinematics at depth on geological time-scales. An alternative is therefore to examine structures in exhumed, inactive fault systems whose tectonothermal history is sufficiently well known to permit inferences on their dynamic evolution.

The term 'fault' is used in this paper for any continuous surface or zone across which there has been displacement, regardless of whether it is a discrete, cataclasitic zone or a ductile, mylonitic shear zone. We therefore use the modifiers 'brittle' and 'mylonitic' to characterize the type of fault. A 'fault system' comprises several faults that are kinematically and temporally related on the crustal scale.

The Periadriatic fault system in the European Alps (Fig. 1) is a natural laboratory for testing hypotheses on the depth-dependence of fault kinematics and dynamics. This exhumed fault system (henceforth abbreviated PFS) trends E–W over a distance of approximately 700 km from northwestern Italy to northern Slovenia. It was active in Tertiary time at the front of an orogenic indenter corresponding to the southern Alps in map view (Fig. 1). Differential exhumation and erosion have exposed sections across this currently inactive fault system at palaeostructural levels ranging from near-surface faulting down to mylonitic shearing at 25–30 km depth. The PFS is the site of several Tertiary granitoid bodies, which are useful markers for constraining the age and kinematics of displacement. In addition, the PFS is transected by four geophysical profiles (TRANSALP, NFP20-E, NFP20-W, ECORS-CROP in Fig. 1), which provide crucial information on its relationship to the deep structure of the Alps.

This paper focuses on three segments of the Periadriatic fault system (boxed areas in Fig. 1) where excellent exposure combined with deep seismic images allow investigation of how strain partitioning during transpression was related to crustal structure. After a brief description of criteria for identifying decoupling, we characterize the structure and kinematics of mylonitic faulting along these segments. These segments are then considered in the broader context of the kinematics and timing of mylonitic faulting and folding along the entire PFS in the Alps, with particular attention paid to the relationship of exhumation and strike–slip faulting to the shape and motion of the southern Alpine indenter. This allows the identification of first-order strain localization patterns that, we argue in the ensuing section, must have been related to decoupling in different levels of the continental crust. This forms the basis for a discussion of how networked folds and shear zones reduce crustal strength while transferring plate-scale forces through the continental lithosphere. The paper concludes with a generic model for partitioned, localized strain and decoupling in orogenic continental crust.

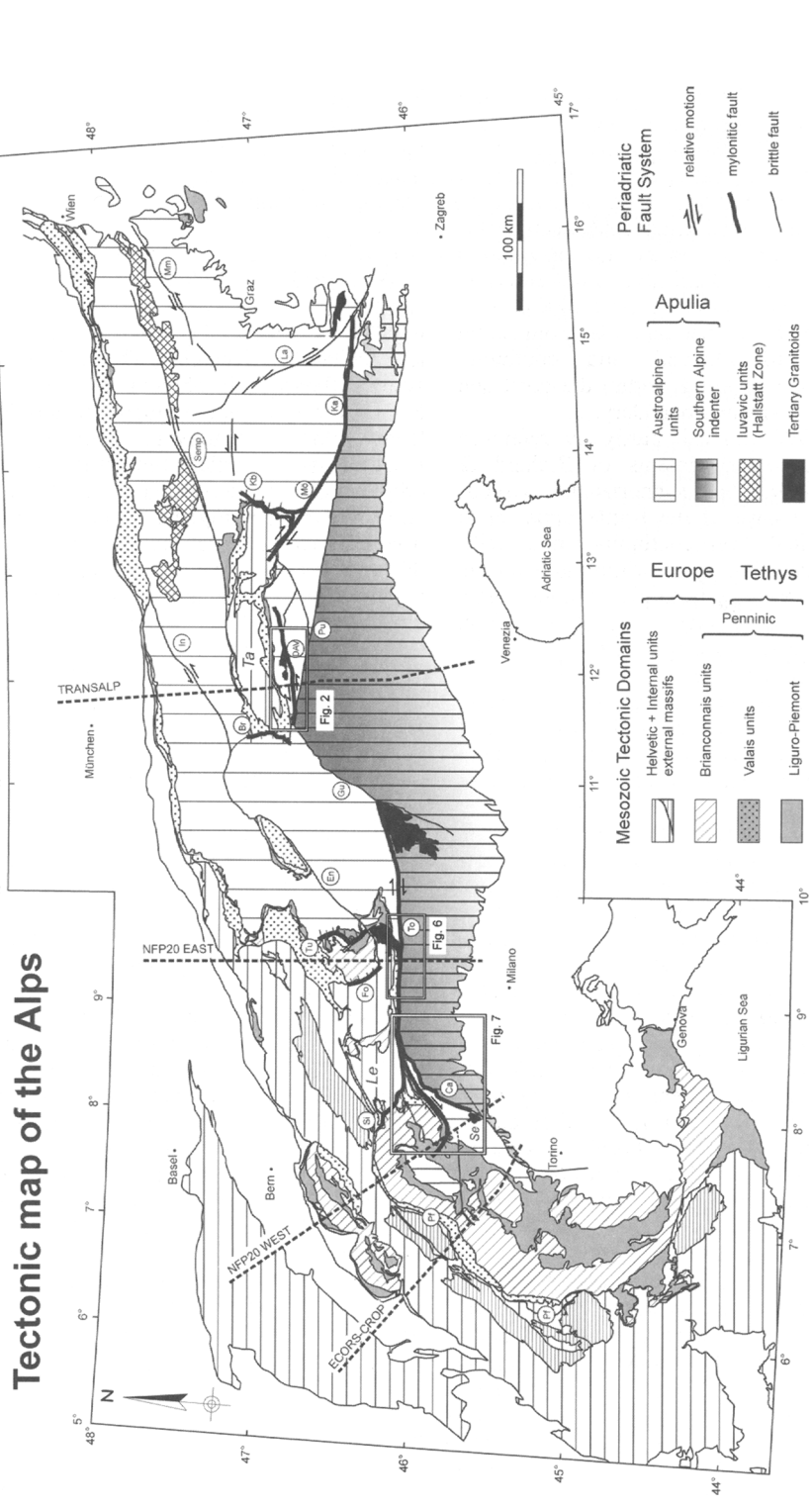


**Fig. 1.** Tectonic map of the Alps with location of study areas (boxes) and four geophysical transects. Se = Sesia zone, Tertiary thermal domes: Ta, Tauern; Le, Lepontine. Mylonitic segments of the Periadriatic fault system (thick lines): Kb, Katschberg extensional fault; Mö, Mölltal fault; DAV, Defereggen–Antholz–Vals fault; Br, Brenner extensional fault; Tu, Turba extensional fault; To, Tonale segment of the Insubric mylonite belt and Tonale brittle fault; Fo, Forcola extensional fault; Ca, Canavese segment of the Insubric mylonite belt; Si, Simplon extensional fault; Pf, Penninic frontal thrust. Segments related to the Insubric mylonite belt are depicted with thicker lines. Brittle faults of the PFS (thin lines): Pu, Pustertal fault; Gu, Giudicarie fault; Ka, Karawanken fault; La, Lavanttal fault; Mm, Murtal–Murztal fault; Semp, Salzach–Ennstal-Mariazell-Puchberg fault; In, Inntal fault; En, Engadine fault. Map modified from own previously unpublished figure, see also Froitzheim *et al.* (1996) and Schmid *et al.* (2004).

## Recognizing mechanical decoupling in rocks

'Coupling' within or between tectonic plates is often implicity equated with the transfer of tectonic stresses, especially shear stress, across active faults. In contrast, 'decoupling' is taken to signify the reduction, or even temporary loss, of shear strength on such surfaces, allowing strain to localize and strain rate to increase. Structural geologists use finite strain gradients or strain discontinuities in rocks to locate faults. Such discontinuities are interpreted in a purely kinematic sense to be the sites of detachment. For detachment to occur, the fault rock must have weakened with respect to the surrounding rock, so the kinematic concept of detachment is related to the mechanical notion of decoupling.

Recent model-based attempts to use curved foliation patterns and uniform shear-sense indicators across mylonitic shear zones as criteria for intracrustal 'attachment' and mechanical coupling (Tikoff *et al.* 2002) are ambiguous because these same structures are ubiquitous in exhumed detachment zones, where offset markers indicate that decoupling must have occurred. Furthermore, structures and finite strain gradients that appear to be continuous at one scale of observation can be discontinuous at other scales.

Therefore, we opted for a combination of two criteria to identify sites of former decoupling in the exhumed Periadriatic fault system: (1) the size of the fault and, where visible, its displacement compared to the sharpness of the strain gradient across it. Faults with widths of $\geq 10^2$ m and/or with comparably large displacements were taken as strong evidence for crustal-scale decoupling. Previously published radiometric ages of fault-related exhumation, or better, ages of syntectonic mineralization within fault rocks, were used to establish whether strain gradients at the margins of a fault system formed during the same time interval as the offset of the markers across this system; (2) the type of fault rock (cataclasite or mylonite). By comparing natural microstructures with microstructures in rock-deformation experiments, we identified the deformation mechanisms and inferred the rheology of the fault rock (criteria in Schmid & Handy 1991). For example, the presence of mylonite or foliated cataclasite is diagnostic of aseismic deformation, whereas pseudotachylite is an indicator of frictional melting and coseismic slip (Sibson 1975; Wenk 1978; Maddock 1983). The mutual overprinting of pseudotachylite and mylonite is interpreted in terms of episodic, coseismic slip that alternated with longer periods of aseismic viscous creep (Hobbs *et al.* 1986; Magloughlin & Spray 1992; McNulty 1995). Thus, we not only identified faults associated with intracrustal decoupling, but also characterized the short-term mechanical stability of the rocks within these faults.

## The Periadriatic fault system

### *Overview*

The PFS comprises many differently aged mylonitic and cataclastic faults within the Tertiary Alpine edifice (Fig. 1). For the purposes of this paper, we restrict our analysis to Oligocene to Miocene parts of the PFS, especially the so-called Insubric mylonite belt, shown with thick black lines in Figure 1. Following Argand (1916) and later Schmid *et al.* (1989), we reserve the term 'Insubric' for Oligo-Miocene deformation in the Alps centered on the PFS. At that time, the Insubric mylonites delimited the warmer, exhuming retro-wedge of the Alpine orogen to the north from colder, southern Alpine units (Schmid *et al.* 1996; Escher & Beaumont 1997). The latter units had cooled to below 300 °C already in Jurassic times (Hunziker 1974; Handy & Zingg 1991), making them hard and brittle during Tertiary Alpine collision (Schmid *et al.* 1989). The Insubric mylonite belt is overprinted by brittle faults, including the sinistral Giudicarie fault (Gu in Fig. 1).

The Insubric segments of the PFS described below occupy parts of the Alpine orogen with quite different characteristics. Whereas the eastern segment (Figs 2 to 5) transects the broadest part of the orogen in the TRANSALP section, the central segment (Fig. 6) occupies the transition from the narrowest part of the orogen along the NFP20-E section to the western termination of the PFS (Figs 7 to 9) along the NFP20-W and ECORS-CROP sections. We will return to these differences in the context of strain partitioning, but first describe the structure of these segments in turn. Readers who are in a hurry can skip the new data in the next three sections and advance directly to the regional synthesis for the Oligo-Miocene PFS (Figs 10, 11) at the end of this chapter.

### *The eastern segment*

*Structure and kinematics.* In map view (Fig. 2), the PFS comprises several faults within a slender wedge of the Austroalpine basement just south of the Tauern Window: (1) the Cima Dura fault (CD), a steeply dipping band of

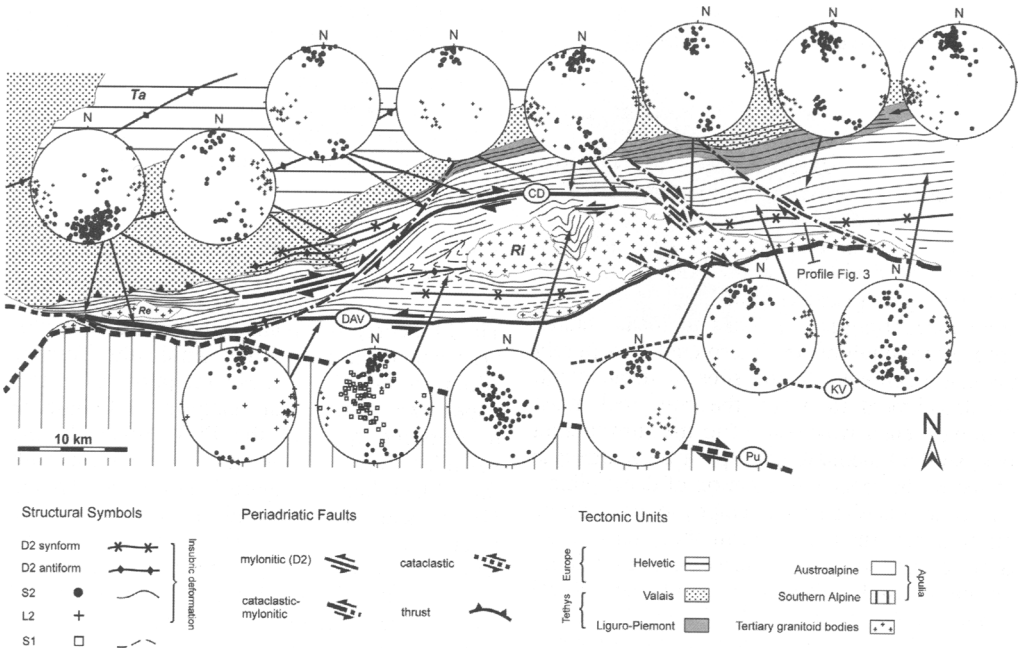


**Fig. 2.** The Periadriatic fault system at the southwestern end of the Tauern window: Structural map. Equal area projections are lower hemispheres. CD, Cima Dura fault; DAV, Defereggen–Antholz–Vals fault; KV, Kalkstein–Valarga fault; Pu, Pustertal fault; Ta, Tauern basement; Ri, Rieserferner pluton; Re, Rensen pluton.

greenschist-facies mylonite; (2) the Defereggen–Antholz–Vals fault (DAV, Borsi *et al.* 1973), likewise a steeply dipping band of greenschist-facies mylonite up to several hundred metres thick that forms the southern limit of Alpine metamorphism (Hoinkes *et al.* 1999); (3) the Kalkstein–Valarga fault (KV), a poorly exposed, discontinuous line of cataclasites; and (4) the Pustertal fault (Pu), a line of cataclasites in basement rocks and low-temperature mylonites in Mesozoic carbonates separating the Austroalpine and southern Alpine basements.

Insubric deformation engendered the main foliation (S2) north of the DAV fault and coincided with activity of the DAV and CD faults, as well as with the intrusion of the Rieserferner pluton (Wagner 2004). The depth of Insubric faulting exposed in this area is about 10 km based on pressure estimates in and around this syntectonic pluton (290–350 MPa, mineral equilibria in the contact aureole, Cesare 1994; 220–510 MPa; Al-in-hornblende geobarometry in massive tonalite, Wagner 2005).

Insubric (F2) folds tighten and become isoclinal as the basement wedge narrows to the west. Their axes are subhorizontal, subparallel to a stretching lineation, L2 (Fig. 2). The main body of the Rieserferner pluton occupies the core of a tight, upright F2 antiform just to the north of the DAV fault (Fig. 3). These Insubric structures are offset by conjugate, mylonitic to cataclastic shear zones that were active under retrograde, greenschist-facies conditions (dashed–dotted lines in Fig. 2).

Several lines of evidence indicate that the Insubric strain field in the Austroalpine basement involved bulk vertical flattening with a strong component of horizontal, ENE–WSW extension. First, the stretching lineation, L2, is subhorizontal and ENE–WSW trending on S2 surfaces, which are generally steeply dipping (Fig. 2). Only in the vicinity of the Rieserferner pluton, where the S2 surfaces are concordant with the pluton's sides and roof (Fig. 3), does the strain field appear to be locally constrictional. Secondly, the largest D2 shear zones are both sinistral (DAV, Kleinschrodt 1987) and dextral (CD, Wagner 2004). This also applies to the somewhat younger conjugate, ductile–brittle faults, which show opposite drag senses of S2 in map view (Fig. 2). Thirdly, the kinematic reconstruction of Frisch *et al.* (1998, fig. 2a) indicates that 12 km of N–S shortening of the Austroalpine basement wedge was associated with an E–W elongation of 53 km. Vertical motion during Insubric (D2) exhumation of

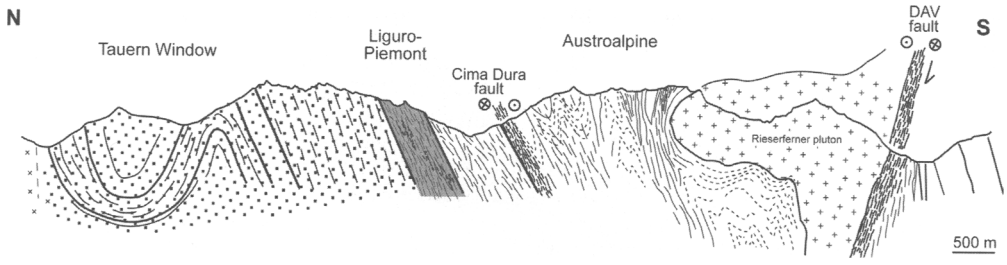


**Fig. 3.** Cross-section of the southwestern part of the Tauern window, including the Rieserferner pluton and DAV fault (modified from Senarclens-Grancy 1965); structures projected into profile section marked by the trace in Figure 2. Symbols as in Figure 2.

the Austroalpine basement was at most 10 km according to the radiometric age constraints discussed below. The axes of N–S shortening and E–W stretching are, respectively, normal and parallel to the E–W striking S2 schistosity. Thus, the principle axes of the bulk finite strain ellipsoid during Insubric faulting were oriented E–W ($+e_1$), vertical ($+e_2$) and N–S ($-e_3$), with elongation taken to be positive. Insubric shearing in the Austroalpine basement wedge was therefore highly coaxial with a non-coaxial component of sinistral shear, mostly accommodated by the DAV fault. A similar pattern of strain partitioning, but involving dextral transpression, occurs along the Mölltal fault at the southeast end of the Tauern window (Fig. 1), as discussed below.

Upper greenschist-facies Insubric mylonites along the contact of Austroalpine and Liguro-Piemont units in Fig. 2a dip subvertically and have a subhorizontal stretching lineation, indicative of ENE–WSW elongation. A similar stretching direction is inferred from subhorizontal L-tectonites in upright, tight to isoclinal folds in the western Tauern window (Lammerer & Weger 1996). Geochronological evidence discussed in the next section suggests that the southern border of the Tauern window was also the site of significant N-side-up exhumation in Miocene time.

*Timing of strike–slip faulting and exhumation.* Age intervals of faulting and exhumation are reconstructed in Figures 4 and 5 from the available geochronological data and from knowledge of the peak temperatures and pressures attained in the fault-bounded crustal blocks. Because metamorphic temperatures in the Austroalpine basement never exceeded about 400 °C in Tertiary time, and the Rb–Sr system in white mica closes to diffusion at about 500 °C (e.g. von Blanckenburg *et al.* 1989), 33–30 Ma Rb–Sr white-mica ages on S2 (Müller *et al.* 2001) (stars in Fig. 4) are interpreted as maximum, formational ages for the onset of strike–slip motion along the DAV fault and CD. The Rb–Sr biotite and K–Ar white-mica cooling age pattern in Figure 4 is interpreted to reflect both fault-related exhumation of basement units north of the DAV fault and the thermal anomaly around the Rieserferner pluton.

Most strike–slip activity of the DAV and CD faults occurred at 33–28 Ma (Müller *et al.* 2001; Wagner 2005). Figure 4 shows that whereas the DAV fault truncates the mica cooling age pattern, the CD fault does not offset the pattern of 14–20 Ma and 20–25 Ma cooling age intervals. This is interpreted to indicate that mylonitic strike–slip faulting lasted until no later than 20 Ma. During and/or after that time, basement units north of and along the DAV fault rose through the 300 °C isotherm. Pseudotachylite locally overprinted by mylonites of the DAV fault (Mancktelow *et al.* 2001; Müller *et al.* 2001) is interpreted as evidence for local, coseismic decoupling during strike–slip mylonitization.

Conjugate, mylonitic-to-cataclastic shear zones that displace the CD and the DAV faults also offset the Rieserferner pluton, but do not seem to affect the 20 Ma mica cooling age isochron (Fig. 4). Most dextral strike–slip movement was taken up along along the brittle Pustertal fault between 20 and 30 Ma ago. This age range is constrained by the coincidence of this fault with 28–29 Ma granitoids (Scharbart 1975) and by a 22–20 Ma $^{40}Ar/^{39}Ar$ crystallization age of pseudotachylite along the fault plane (Müller *et al.* 2001). The Pustertal fault has little, if any, vertical throw (Most 2003). Dextral strike–slip displacement is argued below to amount to some 100 km based on estimates of displacement along the Tonale segment of the Insubric mylonites to the east (see below and Stipp *et al.* 2004).

Figure 5 shows that crustal exhumation migrated from south to north in front of the

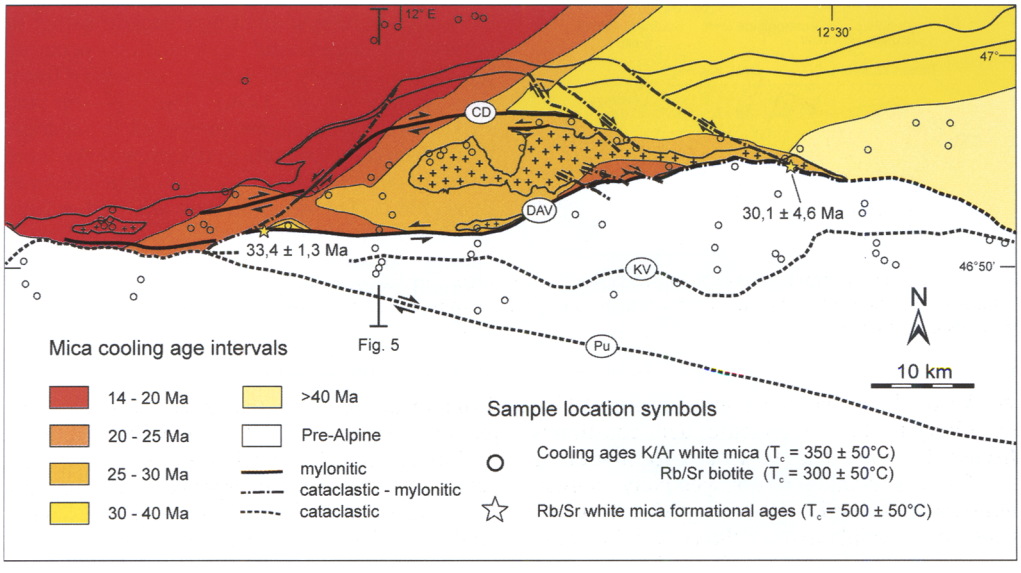


**Fig. 4.** Age interval contours for the area in Fig. 2 constructed from Rb–Sr biotite and K–Ar white-mica ages of Borsi *et al.* (1978*b*) and mica cooling ages contoured in the Tectonometamorphic Age Map of the Alps (Handy & Oberhänsli 2004). Rb–Sr white mica ages are from Müller *et al.* (2000) and Wagner (2004). CD, Cima Dura faults; DAV, Defereggen–Antholz–Vals fault; KV, Kalkstein–Valarga fault; Pu, Pustertal fault.

southern Alpine indenter. For the time interval of 100 to 30 Ma, the KV and DAV faults accommodated, respectively, about 2–3 km and 25 km of vertical exhumation. The DAV fault is therefore interpreted to coincide with the site of an older S-dipping, low-angle normal fault that juxtaposed high-pressure amphibolite-facies assemblages in the north (700 MPa; Stöckhert 1984) with Alpine-unmetamorphosed rocks in the south during Early Tertiary (Müller *et al.* 2001) or even Late Cretaceous time (Borsi *et al.* 1973; Stöckhert 1984; discussion in Mancktelow *et al.* 2001). Oligo-Miocene, N–S shortening during Periadriatic faulting then rotated this extensional fault into its current steep orientation as a sinistral, strike–slip fault.

Most exhumation related to Insubric deformation (*c.* 47 km) is concentrated along the southern border of the Tauern window and occurred between 30 and 5 Ma, with only a modest amount of Insubric exhumation along the DAV fault ($\leq$10 km) at 20 Ma, certainly no later than 10 Ma (Fig. 5 and discussion above). The Austroalpine crust north of and along the DAV fault passed through the 280°C isotherm for the viscous-to-brittle transition in quartz (Stöckhert *et al.* 1999) some 24 to 20 Ma according to zircon fission track ages (Most 2003, and references therein). This late, N-block-up exhumation along the DAV fault involved brittle reactivation of the greenschist-facies mylonites. Apatite fission track ages in this area indicate no significant differential exhumation, or indeed any fault activity, along this part of the Periadriatic fault system after 10 Ma (Stöckhert *et al.* 1999).

Taken together, these age patterns reveal that most E–W stretching of the orogenic crust in front of the southern Alpine indenter began before exhumation through the viscous-to-brittle transition in quartz-rich rocks. The amount of exhumation decreased from west to east in the area of Figure 4 (Borsi *et al.* 1978*a*; Steenken *et al.* 2002), a trend that is possibly related to the westward decrease of orogen-normal shortening (Frisch *et al.* 1998) associated with overall lateral, eastward extrusion of the Eastern Alps (Ratschbacher *et al.* 1991*b*). Most E–W stretching was coeval with the onset of exhumation and rapid cooling of basement rocks in the western Tauern window. E–W stretching and N–S shortening of the Austroalpine basement associated with conjugate, viscous–brittle faulting ceased by 14 Ma at the latest, somewhat before the end of N-block-up exhumation along the DAV fault at 10 Ma.

### *The central segment*

The structure of the Tonale segment of the PFS transected by the NFP20-E section (Figs 1 and 6)

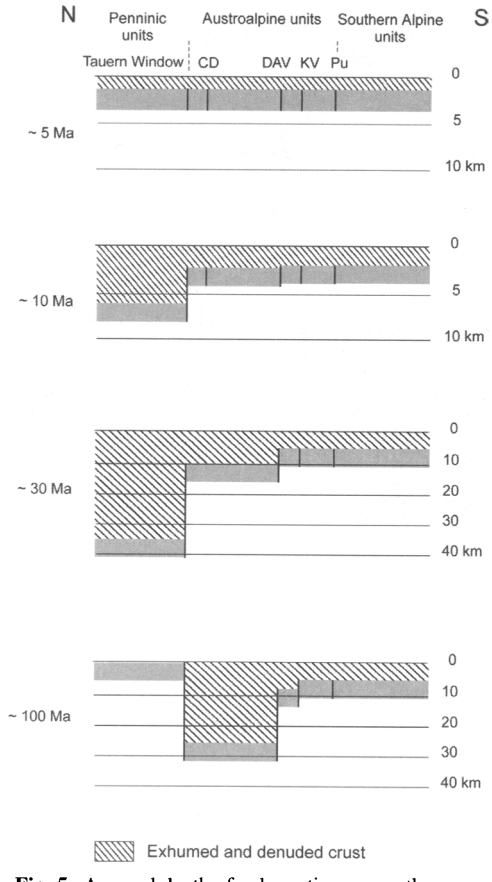


**Fig. 5.** Age and depth of exhumation across the Periadriatic fault system along the N–S oriented profile trace in Figure 4. Peak pressures used to estimate maximum depth of burial are from Stöckhert (1984) and Zimmermann *et al.* (1994). Depths calculated by assuming a geotherm of 30 °C $km^{-1}$ and an average crustal density of 2.8 g $cm^{-3}$. References for radiometric ages: Cesare (1992, 1994), Most (2003), Steenken *et al.* (2002), Stöckhert (1984), Stöckhert *et al.* (1999), and Zimmermann *et al.* (1994).

is relatively straightforward. There, the Insubric mylonite belt comprises a 1 km wide band of retrograde greenschist-facies mylonite that grades northwards into amphibolite-facies mylonite and post-nappe folds of the so-called 'southern steep belt' (Milnes 1974). This steeply N-dipping belt served as a conduit for the syn-tectonic ascent of tonalitic melt that fed the Oligocene Bergell pluton (Fig. 6; Rosenberg *et al.* 1995). South of this pluton, the Insubric mylonites accommodated dextral shear parallel to a subhorizontal stretching lineation (Wiedenbeck 1986; Fisch 1989), whereas within the pluton and to the north, an additional component of N-side-up reverse faulting ('backthrusting' in Alpine parlance) and exhumation occurred parallel to a steeply N-plunging stretching lineation (Berger *et al.* 1996). The dip–slip and strike–slip lineations are preserved in separate, though broadly coeval, northern and southern parts of the Insubric mylonite belt (Schmid *et al.* 1987). The mylonite belt was active from 35 Ma to 20–15 Ma, as constrained by cross-cutting relations with Tertiary intrusives (Bergell pluton–Rosenberg *et al.* 1995, Oberli *et al.* 2004; Adamello pluton–Stipp *et al.* 2004), the successive closure of mineral isotopic systems in the Lepontine dome (Hurford 1986; Villa & von Blankenburg 1992) and the age and uplift rate of Bergell granitoid components in the southern Alpine molasse (Wagner *et al.* 1977; Gunzenhauser 1985; Giger & Hurford 1989). Continued dextral strike–slip motion involved cataclasis along the brittle Tonale fault (Fig. 6) and its continuation to the west, the Centovalli fault (marked Ce in Fig. 7).

The exhumation accommodated by the Insubric mylonite belt ranges from 5 km in the Adamello region (Stipp *et al.* 2004) to a maximum value of 20–25 km at the eastern margin of the Lepontine dome transected by the NFP20-E profile (Fig. 1). Most, if not all, of this exhumation occurred after 28 Ma, when temperatures reached the solidus of the Bergell tonalite at a depth of about 25 km (Oberli *et al.* 2004). Exhumation and cooling rates were highest from 23 to 19 Ma (2.2 mm/a) before slowing to current rates after 19 Ma (0.4 mm/a, Hurford 1986). North of the Insubric mylonite belt, stretching parallel to east–west trending fold axes and mineral lineation affected the folded base of the Bergell pluton during and after intrusion (Davidson *et al.* 1996). Orogen-parallel, E–W extensional exhumation of the Tertiary nappe pile from beneath the Late Cretaceous, Austroalpine nappes was accommodated initially by the Oligocene Turba extensional fault (Nievergelt *et al.* 1996) and then by the 25–18 Ma Forcola extensional fault (Meyre *et al.* 1998) (Fig. 6b).

In the western part of the southern steep belt, the age interval of rapid cooling (18–15 Ma) is somewhat younger than in the eastern part (30–25 Ma, Hurford 1986), suggesting that rapid exhumation migrated from east to west along the E–W striking part of the Insubric mylonite belt (Schmid *et al.* 1989). Extensional exhumation of the western Lepontine dome initiated as early as 35–30 Ma with the onset of dextral transpressional shearing of the Early Tertiary nappe pile (Steck & Hunziker 1994) and continued from 25 to 11 Ma during top-SW, orogen-parallel mylonitic faulting localized

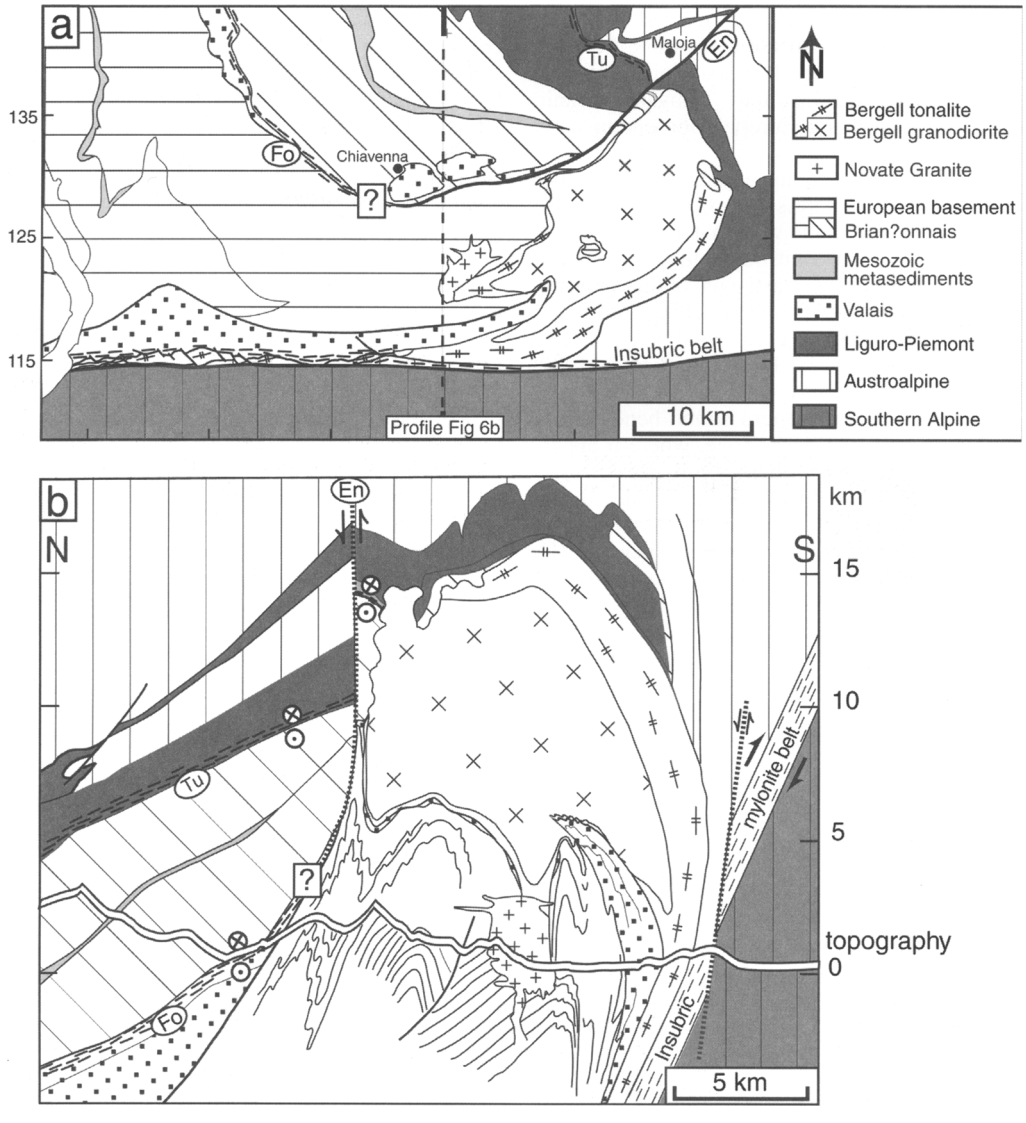


**Fig. 6.** The central segment of the Periadriatic fault system: (**a**) geologic map; (**b**) cross-section with up-plunge projection into the N–S profile line marked A–A′ in Figure 6a (modified from Davidson *et al.* 1996). Dotted line indicates Tonal brittle fault overprinting the Insubric mylonite belt.

along the Simplon extensional fault (Si in Figs 1 and 7; Mancktelow 1992).

### *The western segment*

*Structure and kinematics.* At the western end of the PFS, the Insubric mylonite belt (locally named the Canavese Line or Canavese fault, Ca in Fig. 1) narrows progressively from a width of about 1 km to only several metres as it follows the arcuate border between the basement rocks of the Sesia Zone and the southern Alpine indenter. The surface exposure of the indenter in this area is the Ivrea Zone, whose pre-Alpine mafic and ultramafic rocks can be traced downward in the ECOR-CROP and NFP20-W transects to a SE-dipping wedge of upper mantle rock, the Ivrea Body, that is deeply embedded within the retro-wedge of the Alpine orogen (Nicolas *et al.* 1991; Schmid & Kissling

2000). The Sesia Zone, located on the western side of the Insubric mylonite belt (Se in Fig. 1), is part of the Tertiary Alpine orogenic wedge that includes the Tethyan oceanic units and underlying European basement units (Fig. 7).

The Canavese fault dips moderately to steeply to the NW, and comprises two strands of mylonite (Fig. 7): one in the west that accommodated top–SE to –E backthrusting (plots 5, 7), and a smaller strand in the east with oblique-normal dextral shear parallel to stretching lineations (plot 8). These strands correspond, respectively, to mylonitic belts 2 and 1 of Schmid *et al.* (1987, 1989). In the vicinity of the Tertiary Biella pluton (Fig. 7), the western strand bends to the west and enters the Sesia Zone, where it apparently follows the northern limit of eclogite-bearing rocks. The eastern strand grades to the SW into cataclasites, which are themselves overprinted by cataclasites of the Cremosina fault (Cr in Fig. 7). Yet further to the SW, outside of the map area in Figure 7, the Sesia–Ivrea contact is marked by Late Cretaceous to Early Tertiary, greenschist-facies mylonite (Zingg & Hunziker 1990) and one, possibly two generations of Oligocene or younger cataclasite (Schmid *et al.* 1989). These mylonites are beyond the scope of this paper, as they are related to pre-Insubric extensional exhumation of high-pressure rocks in the Sesia Zone.

As the Canavese fault narrows to the SW, several retrograde greenschist-facies, mylonitic zones fan out westward from the Sesia–Ivrea border and overprint older mylonitic foliations within the Alpine orogenic retro-wedge (Fig. 7). These Insubric splays are steeply dipping, fold and shear zones of up to several hundred metres thickness (Fig. 8) whose mylonitic foliation contains a mostly subhorizontal stretching lineation. The shear sense parallel to this lineation is predominantly dextral, although sinistral shear sense is found within some zones (Fig. 7). In one of these splays, the dextral shear sense is indicated by the left-stepping direction of mylonitic shear zones that merge along strike with en-échelon, upright, tight to isoclinal, non-cylindrical folds with subhorizontal to moderately plunging axes (Fig. 7, plots 2 and 6; Insubric fold zone in Fig. 8). In other locations, the shear zones skirt narrow synforms that contain klippen of pre-Alpine rocks belonging to the Upper Unit of the Sesia Zone (Figs 7 and 8, 'Seconda Zona Dioritica Kinzigitica' or II ZDK of Gosso *et al.* 1979). Along the sides of some of these klippen, the mylonitic foliation dips moderately and the stretching lineation rotates into a direction consistent with shear upward and outwards from the synformal cores (e.g. plot 6 in Fig. 7).

The southern steep belt, including prominent S- to SE-vergent post-nappe folds like the Vanzone antiform (Va in Fig. 7), gradually disappears from NE to SW as it trends away from the arcuate Sesia–Ivrea border and acquires a progressively shallower southeastward dip in the western part of Figure 7. A dextral band of retrograde, amphibolite- to greenschist-facies mylonite follows the contact of Liguro–Piemont and Brianconnais units marking the narrow southern limb of the Vanzone antiform (plots 3 and 4 in Fig. 7). In the axial trace of this antiform at the SW end of the Monte Rosa nappe, the mylonitic foliation dips moderately to the SSW (Fig. 7) with a SW-dipping stretching lineation (Steck & Hunziker 1994) This indicates NE–SW extension parallel both to the SW-plunging axis of the Vanzone antiform and to NE–SW trending L-tectonite fabrics in the core of this antiform (Reinhardt 1966). Going to the NE along the steep belt in Figure 7, this same mylonitic band steepens and partly overprints the retrograde greenschist-facies mylonitic foliation of the Gressoney fault (Fig. 8). The Gressoney fault (plot 1 in Fig. 7) has been interpreted as a mid- to late Eocene, low-angle normal fault that accommodated top-SE shear (Wheeler & Butler 1993) prior to Insubric deformation.

*Age of faulting and exhumation.* The coincidence of Insubric mylonitic splays emanating westward from the southern Alpine indenter with the disappearance to the southwest of both the Insubric mylonite belt and the southern steep belt suggests a kinematic link between Tertiary shortening, exhumation and NE–SW-directed, orogen-parallel extension in the Western Alps. Establishing this link requires accurate dating of the minerals defining the mylonitic foliations in Figure 7.

The tectono-metamorphic age map in Figure 9 shows the distribution of selected Rb–Sr and K–Ar white-mica ages in the literature for areas where the main foliation has a clear relative age (based on cross-cutting relationships) and an unambiguous shear sense (based on kinematic indicators). Only samples for which there was no discernable evidence for inherited effects of pre-Alpine or high-pressure metamorphism are plotted in this figure. Where dated samples were lacking, we extrapolated and interpolated age results parallel to the strike of foliations that were structurally and kinematically continuous. The resulting age map allows one to distinguish mylonites of the

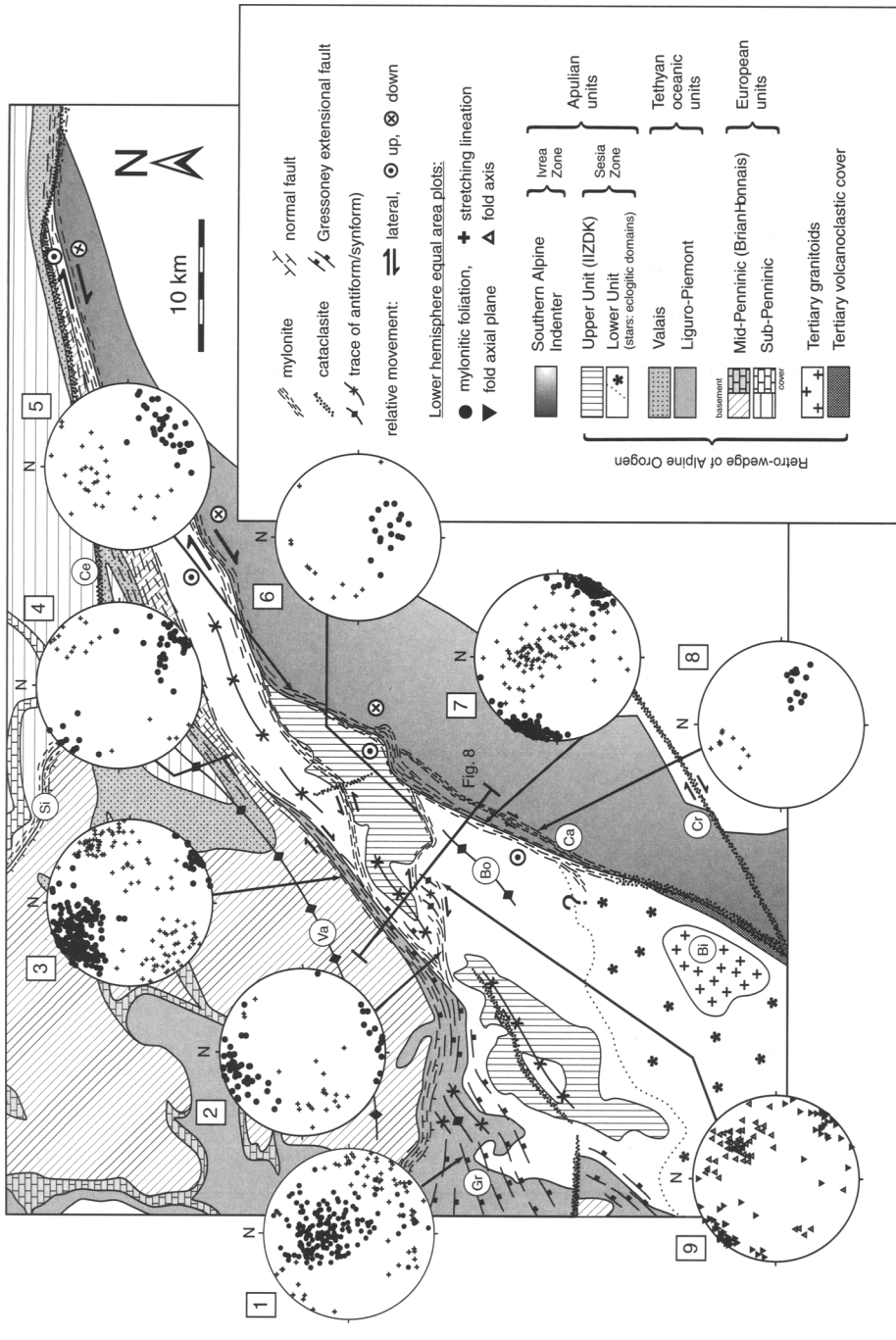


**Fig. 7.** Structural map of the western end of the Periadriatic fault system. Equal area projections are lower hemispheres with own structural data, for NW parts of the Gressoney extensional fault with data from Reddy *et al.* (1999, 2003), and for core and crest region of the Vanzone antiform with data, respectively, of Reinhardt (1966) and Steck & Hunziker (1994). Numbering of projections is cited in the text. Ca, Canavese segment of the Insubric mylonite belt; Ce, Centovalli fault; Cr, Cremosina fault; Gr, Gressoney extensional fault; Si, Simplon extensional fault; Va, Vanzone antiform; Bi, Biella granite pluton; Bo, Boccioletto antiform.

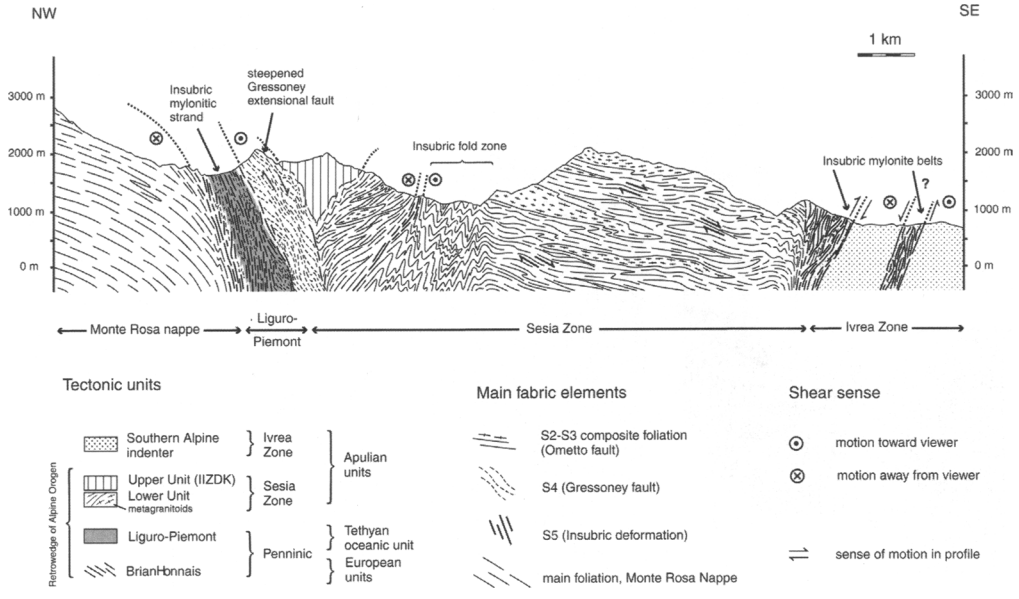


**Fig. 8.** Cross-section parallel to the trace in Figure 7.

southern steep belt and the Canavese fault from Early Tertiary, extensional faults (Ometto and Gressoney faults in Fig. 9). The Ometto and Gressoney extensional faults contributed to the exhumation of Late Cretaceous and Early Tertiary eclogites, respectively, in the Sesia Zone and in the underlying ophiolitic and European basement units.

Dextral shearing under amphibolite- to greenschist-facies conditions in the southern steep belt is inferred to syn-date Vanzone backfolding and related NE–SW, axial extension, based on the structural relations above. Steck & Hunziker (1994) argue that dextral shearing occurred some 35–25 Ma. The upper age limit for this mylonitization is given by 25–29 Ma U–Pb, Rb–Sr and $^{40}Ar/^{39}Ar$ ages of syn- to post-mylonitic dykes (locations in Fig. 9; Romer *et al.* 1996; Schärer *et al.* 1996). Vanzone backfolding affected the pattern of 38 Ma Rb–Sr white mica and 24–20 Ma Rb–Sr biotite cooling ages (age contours in Fig. 9; Steck & Hunziker 1994), but not the pattern of zircon fission track ages at 15 Ma, the time when temperatures fell below 225–240 °C (Hunziker *et al.* 1992). Therefore, this backfolding probably occurred between 35 and 20 Ma.

W-side-up backthrusting and dextral strike–slip in greenschist-facies, Insubric mylonites of the Canavese fault are dated at 26–19 Ma by K–Ar formational white-mica ages (Zingg & Hunziker 1990). This age range may extend back to 30 Ma based on the occurrence of synmylonitic dykes with close mineralogical and geochemical affinity to the Bergell granitoids (Reinhardt 1966; Schmid *et al.* 1987). Within the limits of age resolution, the Insubric mylonitic splays in the northeastern part of the Sesia Zone fall in the same age range; certainly, these splays post-date the cessation of Gressoney extensional faulting by 36 Ma (Reddy *et al.* 1999 and references therein), but precede the transition from viscous to brittle deformation in quartz-rich rocks before cooling to the 225–240 °C closure temperature for fission tracks in zircon at about 15 Ma (Hunziker *et al.* 1992). The difference in closing temperatures of the Rb–Sr white mica and FT zircon systems indicates that the temperature in the NE Sesia Zone and adjacent Penninic units decreased by some 200–300 °C between 35 and 15 Ma. Thus, exhumation due to Insubric folding and backthrusting in this area amounted to about 7–14 km for assumed geothermal gradients of 20–30 °C.

Insubric exhumation is much more modest ($\leq$3 km) in the vicinity of the Biella pluton (Fig. 7) and to the southwest, based on the occurrence of 45–30 Ma zircon FT ages and 15–8 Ma apatite FT ages in that area (Hurford *et al.* 1991). This is corroborated by several observations suggesting that the southwestern part of the Sesia Zone was at or near the surface already prior to, or during, Oligocene time: (1) the Oligocene Biella pluton is a shallow intrusion ($\leq$5 km, Rosenberg 2004) and truncates the foliation of rocks with Late Cretaceous, Rb–Sr white

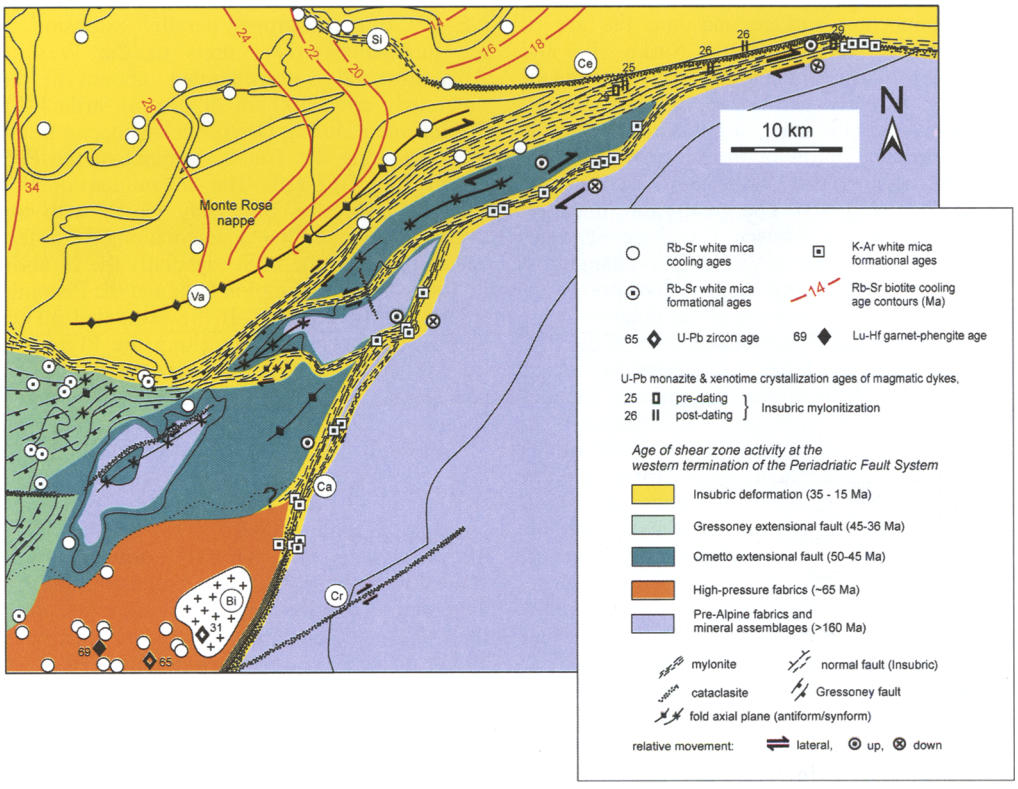


**Fig. 9.** Tectonometamorphic age map of the western end of the Periadriatic fault system based on geochronological data of Duchêne *et al.* (1997), Hunziker (1974), Hunziker *et al.* (1992), Inger *et al.* (1996), Reddy *et al.* (1996, 2003), Romer *et al.* (1996), Rubatto *et al.* (1999), Ruffet *et al.* (1997), Schärer *et al.* (1996), Wemmer (1991), Zingg & Hunziker (1990). Contours of Rb–Sr cooling ages from Steck & Hunziker (1994). Outline of tectonic units corresponds to Figure 7.

mica (Fig. 6) and Early Tertiary, Rb–Sr biotite cooling ages (Hunziker *et al.* 1992); (2) the Oligocene volcanoclastic cover of the Sesia Zone includes boulders of exhumed, Late Cretaceous (Duchêne *et al.* 1997; Rubatto *et al.* 1999) eclogite (Bianchi & Dal Piaz 1963). Subsequent rotation of the Sesia–Ivrea contact into its current steep attitude along the Boccioleto antiform (Bo in Fig. 7; Steck & Hunziker 1994) cannot have involved significant post-Oligocene vertical displacement, because Oligocene igneous rocks in the internal part of the Sesia Zone (e.g. Biella pluton, volcanoclastics, Fig. 7) are exposed at about the same altitude as Tertiary intrusives in the Ivrea Zone (Miagliano tonalite; Carraro & Ferrara 1968).

### *Synthesis of structural, kinematic and age relations of Insubric faulting along the PFS*

The structure, kinematics and age ranges of mylonitic faults making up the PFS are summarized in Figures 10 and 11 from results and literature cited above and in the figure captions. In Figure 10, only mylonitic foliations and stretching lineations from Oligo-Miocene segments of the PFS are included in the projections. The distribution of these fabrics with respect to the orientation of the indenter surface lends insight into how strain was partitioned on the orogenic scale in front of the southern Alpine indenter. The black arrows indicate the Oligo-Miocene motion of the southern Alpine indenter relative to a stable Europe, as determined by palaeomagnetic studies (e.g. Dercourt *et al.* 1986; Dewey *et al.* 1989).

Post-nappe folding and NE–SW-directed axial extension in the Western Alps (Fig. 10) was broadly coeval with N-side-up exhumation and dextral strike–slip along the PFS at the east–west trending, northern surface of the southern Alpine indenter in the Central Alps (Fig. 11). At the NW corner of the indenter, mylonite belts that accommodated dextral strike–slip splay westwards, away from the

angular indenter surface and into the arc of the Western Alps (Fig. 10). Strike–slip and dip–slip motion along and in front of the indenter were strongly partitioned, as indicated by the point-maxima stretching lineation patterns in Insubric mylonites of the western Canavese segment and in the northeastern part of the Sesia Zone (Fig. 10). The great-circle lineation pattern along the eastern Canavese segment (Fig. 10) is interpreted to reflect changes in this partitioning during dextral, transpressional flow around the arcuate tip of the indenter.

The Tonale and Pustertal segments of the PFS are estimated to have accommodated about 100 km of dextral strike–slip motion parallel to subhorizontal stretching lineations (To in Fig. 10; Schmid & Kissling 2000). Total values of dextral displacement range from 110 km (Lacassin 1989) to 150 km (Laubscher 1991), but post-Oligocene movement probably amounted to no more than 30 km (Müller *et al.* 2001). Most, if not all, of this limited, post-Oligocene movement was probably accommodated by the aforementioned brittle faults that overprint the Insubric mylonite belt. The PFS, including the Insubric mylonites, also accommodated a poorly constrained amount of Tertiary N–S shortening to the north of the southern Alpine indenter. Regarded perpendicular to the current E–W trend of the PFS, this shortening varies along strike from a maximum post-Oligocene value of about 113 km in the TRANSALP transect (Frisch *et al.* 1998) to a post-Eocene estimate of 63–71 km parallel to the NFP20-E transect (Schmid & Kissling 2000). Along the Tonale segment, part of this N–S shortening was taken up by S-directed backthrusting parallel to steep, N-plunging stretching lineations in the Insubric mylonite belt (Fig. 10).

Orogen-parallel extension along low-angle normal faults beginning in Oligocene time exhumed progressively deeper units of the folded, Early Tertiary nappe pile. The Simplon and Forcola faults are largely responsible for oblique, NE–SW directed extensional unroofing of the western Lepontine dome by late Miocene time (lineation poles and open arrows in Fig. 10, ages in Fig. 11). The Turba fault at the eastern end of the Lepontine dome is the structurally highest of these extensional faults and was active already in early Oligocene time (Fig. 11). Along the Tonale segment of the Insubric mylonite belt, dextral strike–slip motion outlasted N-side-up exhumation and continued under brittle conditions into Mio-Pliocene time (Fig. 11).

The structural and age relations above support the idea that coeval NW–SE shortening and NE–SW-directed orogen-parallel extension in the internal basement units of the Western Alps absorbed a considerable amount of the previously cited 100 km of dextral strike–slip displacement during Oligocene–Miocene transpression along the Tonale segment of the PFS (arrows in Fig. 10). The magnitude of this NE–SW extension obviously varies with the age and amount of displacement along the different segments of the PFS, especially the Insubric mylonite belt, the Simplon fault and the Penninic frontal thrust (Fig. 10). If the estimated 30 km of post-Oligocene motion along the PFS cited by Müller *et al.* (2001) were taken up by 25–11 Ma Simplon extensional faulting (32–36 km displacement estimates of Grasemann & Mancktelow 1993; Wawrzyniec *et al.* 2001), then the remaining 70 km of pre-Miocene strike–slip displacement along the PFS were probably accommodated by 35–20 Ma, NW–SE shortening and NE–SW orogen-parallel extension of the Monte Rosa basement unit that structurally overlies the Simplon extensional fault. This estimate is close to the maximum 80 km of NE–SW extension proposed by Steck and Hunziker (1994) for the entire Tertiary nappe edifice, including the Simplon fault. Greater amounts of post-Oligocene shortening along the Penninic frontal thrust in the Western Alps, for example, 60 km proposed by Schmid & Kissling (2000), lead to more modest estimates of basement shortening and related NE–SW extension at the western termination of the Insubric mylonite belt.

In the Eastern Alps, sinistral shear of the orogenic crust north of the DAV fault at the southwestern margin of the Tauern window (Fig. 10) was transitional in space and time to doming of the western Tauern window (Fig. 11). This doming involved extension parallel to colinear ENE–WSW trending axes of km-scale, upright folds and colinear stretching lineations (Lammerer & Weger 1996), as indicated by the single-girdle pattern of the foliation poles and the point-maximum of the lineations (Fig. 10). These patterns are consistent with sinistral transpression with a strong component of ENE–WSW stretching. This was coeval with N-side-up exhumation, which largely ended along the DAV fault by 20 Ma but migrated northward into the western Tauern window (Fig. 11). Doming was then transitional to ENE–WSW extension parallel to the stretching lineation in mylonite of the overlying Brenner extensional fault (Figs 10 and 11). The Mölltal fault at the southeastern margin of the Tauern window shows a similar, perhaps somewhat younger evolution to the DAV fault, but with

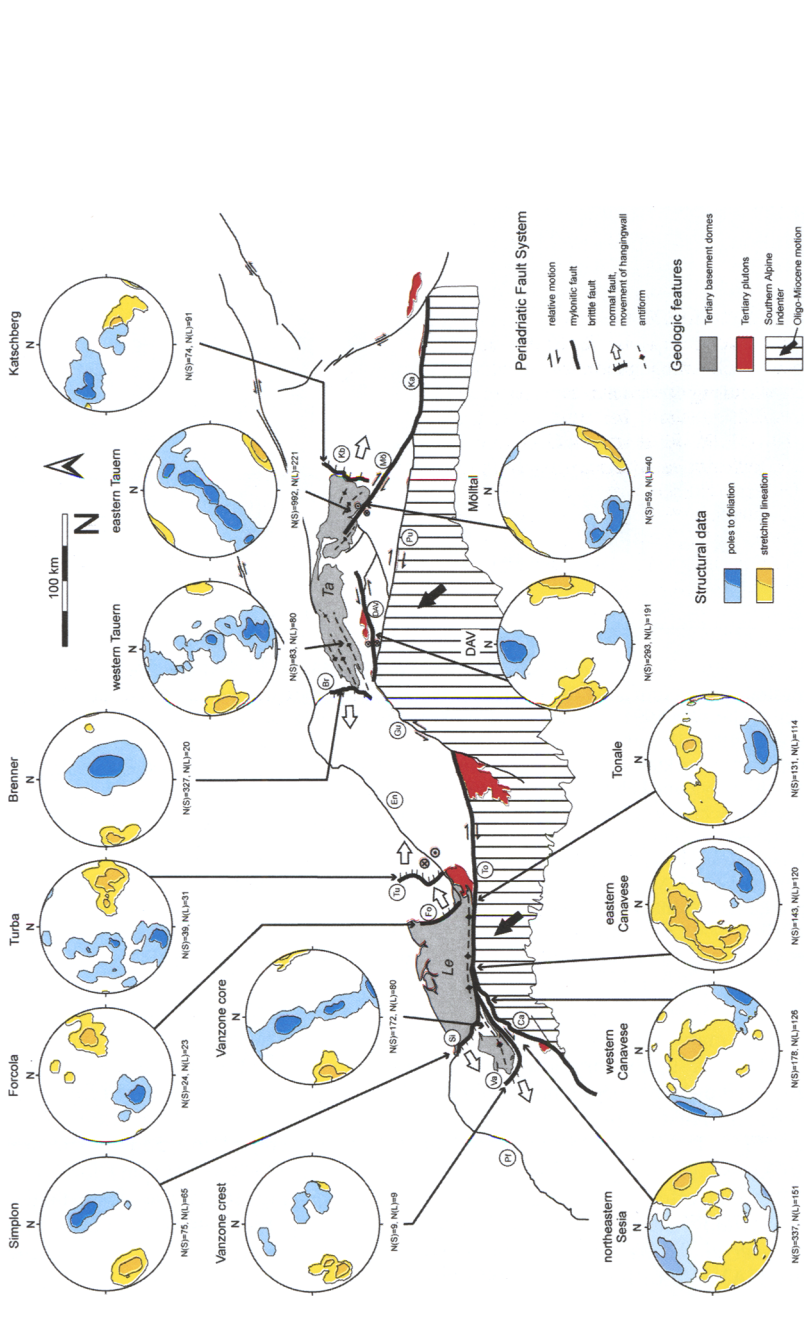


**Fig. 10.** Planar and linear fabric elements along the Periadriatic Fault System. Lower hemisphere equal area projections show contoured poles to mylonitic foliation (blue) and stretching lineation (yellow); contour intervals are multiples of a uniform distribution depending on *N*, the number of measurements. Symbols and abbreviations from Figure 1. Structural data from the following sources: Katschberg extensional fault (Figs 3a, b of Genser & Neubauer, 1989), Mölltal fault (Fig. 2 of Kurz & Neubauer 1996), eastern Tauern folds (Fig. 2 of Kurz & Neubauer 1996, Fig. IV-13 of Cliff *et al.* 1971), DAV, Defereggen–Antholz–Vals fault (Fig. 2 above), western Tauern folds (Fig. 6 in Lammerer & Weger 1996), Brenner extensional fault (Axen *et al.* 2001), Tonale segment of Insubric mylonite belt (Fig. 10b of Berger *et al.* 1996), Turba extensional fault (Fig. 4 of Nievergelt *et al.* 1996), Forcola extensional fault (Fig. 2 of Meyre *et al.* 1998), Simplon extensional fault (Fig. 22 of Mancktelow 1990), western Canavese segment of Insubric mylonite belt (Fig. 7 above, mylonite belt 2 of Schmid *et al.* 1989), eastern Canavese segment (Fig. 3 of Schmid *et al.* 1987), core of Vanzone antiform (fig. 3a of Reinhardt 1966), crest of Vanzone antiform (fig. 3 of Steck & Hunziker 1994). Black arrows indicate motion of the southern Alpine indenter with respect to stable Europe.

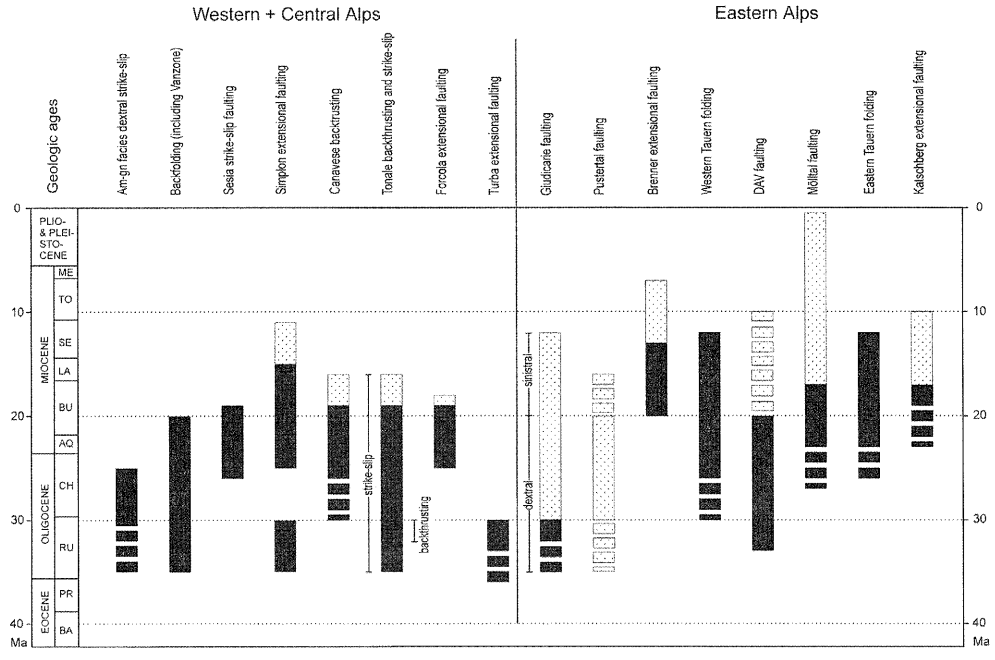


**Fig. 11.** Age ranges of the Periadriatic fault segments. Stippled, brittle deformation; solid, mylonitic deformation; striped pattern, poor age constraints on deformation. Sources: Amphibolite- to greenschist-facies, dextral strike–slip in the southern steep belt (Steck & Hunziker 1994; Romer *et al.* 1996; Schärer *et al.* 1996). Backfolding (this paper; Steck & Hunziker 1994; Hurford *et al.* 1991; Hunziker *et al.* 1992), strike–slip faulting in the northeastern Sesia Zone (this paper), Simplon extensional fault (Mancktelow 1992; Grasemann & Mancktelow 1993; Steck & Hunziker 1994), Canavese segment of the Insubric mylonite belt (this paper; Zingg & Hunziker 1990), Tonale segment of the Insubric mylonite belt (Berger *et al.* 1996; Schmid *et al.* 1989; Schmid *et al.* 1996; Stipp *et al.* 2004), Forcola extensional fault (Meyre *et al.* 1998), Turba extensional fault (Nievergelt *et al.* 1996; Schmid *et al.* 1996), Giudicarie fault (Müller *et al.* 2001; Stipp *et al.* 2004), Brenner extensional fault (Frisch *et al.* 2000; Fügenschuh *et al.* 1997), Western Tauern folding (compilations of Fügenschuh *et al.* 1997; Most 2003), Defereggen–Antholz–Vals fault (this paper; Borsi *et al.* 1978*a*, *b*; Müller *et al.* 2001), Pustertal fault (Müller *et al.* 2001; Stipp *et al.* 2004), Mölltal fault (Kurz & Neubauer 1996; Reddy *et al.* 1993; Inger & Cliff 1994), Eastern Tauern folding (Cliff *et al.* 1985; Reddy *et al.* 1993), Katschberg extensional fault (Dunkl *et al.* 2003; Frisch *et al.* 2000); time-scale according to Harland *et al.* (1989).

the opposite shear sense in map view (Figs 10 and 11). It accommodated N-side-up exhumation combined with dextral strike–slip shear that offsets the contact between Austroalpine and Liguro-Piemont units (Fig. 1). The Mölltal fault trends parallel to km-scale, upright folds (Kurz & Neubauer 1996) that effected doming of the eastern Tauern window at 26–12 Ma (Cliff *et al.* 1985; Reddy *et al.* 1993). Like the large folds north of the DAV fault, these folds have constrictional fabrics in their cores (Cliff *et al.* 1971) and define great-circle foliation girdles and subhorizontal point-maxima lineation patterns (Fig. 10). Such fabrics are diagnostic of NW–SE directed extension parallel to the fold axes, leading Kurz & Neubauer (1996) to interpret the Mölltal fault as a stretching fault in the sense of Means (1989). The continued activity of the Mölltal fault under brittle conditions to recent times is attributed to Plio-Pleistocene dextral motion along the Karawanken fault (Ka in Fig. 1; Polinski & Eisbacher 1991). The Katschberg extensional fault at the eastern end of the Tauern window accommodated top-SE motion parallel to a stretching lineation (Fig. 10; Genser & Neubauer 1989), opposite to the top-WSW extension along the broadly coeval Brenner fault at the western end of the Tauern window.

The similar structural evolution and conjugate geometry of the faults and related folds at opposite ends of the Tauern window suggests that they effected orogen-parallel extension and exhumation of the Early Tertiary nappe pile in the Tauern window (open arrows in Fig. 10). Estimates of this extension range from a minimum of about 37 km (displacement estimates of 20 km and 17 km, respectively, for the

Brenner and Katschberg extensional faults; Behrmann 1988; Selverstone 1988; Genser & Neubauer 1989) to a maximum of 160 km (Frisch *et al.* 1998), depending on the structural markers used and assumptions made about the amount of erosion. Tertiary E–W stretching and exhumation of the Tauern thermal dome in the Eastern Alps has been attributed to simultaneous northward motion of the southern Alpine indenter and lithospheric thinning beneath the Pannonian basin during eastward, hinge roll-back subduction in the Carpathians (e.g. Royden & Burchfiel 1989; Ratschbacher *et al.* 1991*a*). As pointed out in the next section, N–S to NNE–SSW directed shortening and E–W stretching of the Eastern Alps during oblique indentation implies decoupling along the dextral Pustertal fault marking the front of the southern Alpine indenter (Pu in Fig. 10).

The brittle Pustertal fault was active in Oligo-Miocene times before being offset by sinistral strike–slip motion along the Giudicarie fault (Fig. 11). The kinematic history of the Giudicarie fault is controversial, with some authors interpreting it as an inherited restraining bend in the PFS with only minor sinistral displacement (Mancktelow *et al.* 2001; Viola *et al.* 2001) and others arguing that it was originally E–W oriented and rotated into its current NNE–SSW trend while accommodating some 70 km of sinistral offset from 20 to 12 Ma (Fig. 11; Schmid *et al.* 1996; Stipp *et al.* 2004). We favour the latter scenario, because the amount of Tertiary, E–W shortening in the vicinity of the Giudicarie fault is too small ($\leq$30 km) to accommodate the aforementioned 70 km of pre-Miocene, dextral strike–slip displacement along the Tonale segment of the Insubric mylonite belt. Also, sinistral motion of the Giudicarie fault is kinematically linked to Miocene, S-directed thin-skinned folding and thrusting beneath the southern Alpine Molasse (Pieri & Groppi 1981; Laubscher 1996; Prosser 1998; Schönborn 1999). Therefore, prior to 20 Ma, the Insubric mylonite belt in the Western and Central Alps and the Pustertal fault in the Eastern Alps were part of a continuous, E–W trending lineament along the northern edge of the southern Alpine indenter. Lateral stretching and eastward extrusion of the Eastern Alps in front of the southern Alpine indenter continued well into late Miocene time along a conjugate array of brittle, strike–slip faults (In, Semp, Mm, La, Mö, Pu in Fig. 1; e.g. Ratschbacher *et al.* 1991*b*).

The synthesis above reveals that for all parts of the PFS, lateral extension and exhumation of basement nappes along and in front of the indenter surface involved constrictional folding and mylonitic faulting. This occurred when pre-existing foliations rotated into a steep orientation, thereby facilitating strike–slip and dip–slip displacements. Folding and strike–slip faulting were transitional in space and time to low-angle normal faulting at the viscous-to-brittle transition. The orientations of these mylonitic faults and folds with respect to the indenter surface reflect significant differences in intracrustal decoupling patterns, as discussed in the next section.

## Intracrustal decoupling along the Periadriatic fault system

The correlation of strain gradients, displacements and ages of fault activity along the various mylonitic segments of the PFS in the previous section now allow us to identify decoupling zones as defined at the outset of this paper. These zones are related to the subsurface structure of the Alpine orogen, depicted in a block diagram of the Western Alps in Figure 12. This diagram was constructed by combining the geometry and kinematics of the PFS mapped at the surface with subsurface images of the lower crust and upper mantle along the ECORS-CROP and NFP20-W geophysical transects in Figure 1. It reveals that decoupling within the crust occurred along two types of heterogeneity: (1) inherited lithological and/or thermal discontinuities (coloured red), especially the surface of the southern Alpine orogenic indenter; and (2) strain-induced heterogeneities (coloured yellow) within the orogenic crust in front of the indenter.

### *Decoupling at the indenter surface*

The most prominent decoupling zone was the interface between the cold, brittle pre-Alpine rocks of the orogenic indenter and the warm, amphibolite-facies rocks of the Early Tertiary nappe pile. This surface was the locus of exhumation and strike–slip motion within the retro-wedge of the Alpine orogen. The prevalence of mylonite along this surface indicates that decoupling involved largely aseismic, viscous creep. Pseudotachylite zones in the Insubric mylonite (e.g. DAV fault; Mancktelow *et al.* 2001) and in the adjacent southern Alpine rocks (Ivrea Zone; Zingg *et al.* 1990) are modest in extent (cm to m length) and are therefore interpreted to represent only short periods of embrittlement and limited coseismic slip along the indenter surface.

The concentration of strain along the indenter surface is most pronounced along the Tonale and

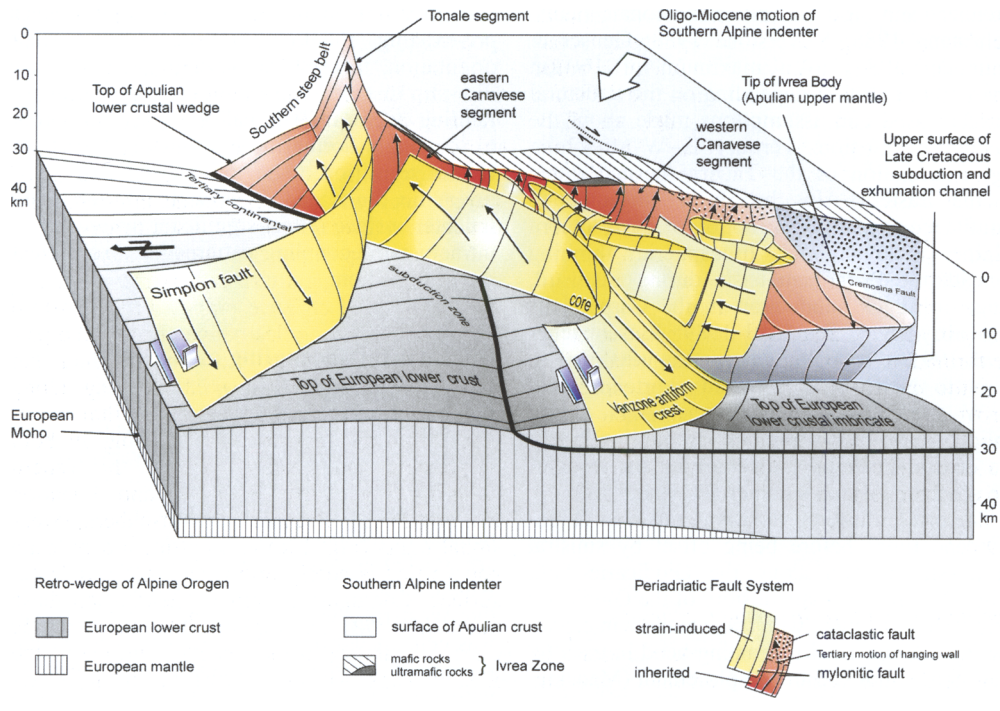


**Fig. 12.** Block diagram of mylonitic segments of the Periadriatic fault system in the Central and Western Alps as viewed towards the southeast. To simplify the view, basement units are stripped away. Decoupling localized along inherited, lithological and thermal heterogeneities (red surfaces) or along strain-induced, rotated anisotropies (yellow surfaces). Base of the lower crust adopted from subsurface interpretations of Schmid *et al.* (1996) and Schmid & Kissling (2000) for the NFP20-E, NFP20-W and ECOR-CROP transects (locations in Fig. 1).

Canavese fault segments, where the Insubric mylonites follow the angular, leading edge of the Ivrea Body. None of the faults extend into the mantle, but root at, or somewhere above, the top of the lower crust (Fig. 12). The lower crust of both the lower (European) and upper (Apulian) plates consists of mafic rocks, based on its high seismic velocity and seismic reflectivity (Valasek & Müller 1997). Beneath the Central Alps, the Apulian lower crust forms an indented wedge that is replaced to the west by an imbricated wedge of lower European crust (Schmid & Kissling 2000). This wedge-like geometry suggests that the lower crust and upper mantle were very strong during Oligo-Miocene indentation and confirms the view previously expressed for the individual transects that the base of the viscous, quartz-rich crust was a first-order decoupling horizon in the Alps.

Upper mantle structures like the Ivrea Body are by no means restricted to the Western Alps, having been imaged beneath the trace of several active transpressive faults, including the Alpine fault zone on the Tasmanian–Pacific plate boundary (e.g. Oliver & Coggon 1979), the San Andreas fault on the Pacific–North American plate boundary (Teyssier & Tikoff 1998), and the El Pilar–Coche Fault Zone on the Caribbean–South American plate boundary (Teyssier *et al.* 2002). The rheological contrasts associated with disparate MOHO depths across such active transpressional boundaries are accentuated by high, lateral thermal gradients, especially where the faults along these boundaries accommodate crustal exhumation or serve as conduits for the rapid ascent of melt. In the case of the PFS, progressive cooling and hardening of the viscously deforming hangingwall adjacent to the southern Alpine indenter is a possible explanation for the migration of exhumation into the retro-wedge of the Alpine orogen.

No pseudotachylite has been found so far along Insubric mylonitic zones away from the surface of the southern Alpine indenter. The concentration of pseudotachlyite at the indenter surface may reflect the relative strain rate and/or width of these mylonitic fault zones when they were active under amphibolite- to greenschist-facies conditions. Chester (1995) argues that seismic instabilities are suppressed in wider zones

because local flow perturbations are damped, thereby favouring velocity-strengthening behaviour. This is especially true of mylonitic faults, where the dominant deformation mechanisms (dislocation creep, diffusion creep) are rate-dependent and the rocks strengthen with increasing strain rate (Scholz 1990). At comparable displacement rates, narrower faults deform at higher strain rates, which favour a switch to velocity-weakening, in some cases leading to seismic instability (Chester 1995). The actual width of the Insubric mylonite belt at any given time during its activity, especially during pseudotachylite formation, is not known. It was probably less than the present 1–2 km thickness, especially during the latter stages of exhumation when lateral thermal gradients across the fault zone led to a strong localization of strain in ultramylonites derived from relatively cold protoliths (>200 °C) of the southern Alpine indenter (Zingg *et al.* 1990).

### *Decoupling within the orogenic crust*

The mylonitic faults in the orogenic crust in front of the southern Alpine indenter represent strain-induced mechanical heterogeneities (yellow surfaces in Fig. 12). Decoupling below the viscous-to-brittle transition was due to the progressive folding and rotation of older faults and foliations into orientations which became conveniently oriented for mylonitic shearing (Fig. 10). Both the Gressoney extensional fault in the Western Alps and the extensional predecessor to the DAV fault in the Eastern Alps were steepened, then reactivated as mylonitic strike–slip faults. The progressive reorientation and reactivation of such pre-existing anistropies represent the strain-dependent growth of new mechanical phases.

Insight into the kinematic and dynamic significance of such anisotropies for decoupling within the orogenic crust is gained from the orientational distribution of foliation (Sm) poles and stretching lineations (Ls) for mylonitic faults of the PFS in Figure 13. The pole diagrams in this figure were constructed by reorienting the contoured foliation and stretching lineation poles for the faults in Figure 10 into a common coordinate system with the indenter surface along the PFS as a vertical reference plane. In Figure 13, this plane is the equatorial line of all the pole diagrams. The local orientation of the indenter surface obviously varies along strike of the PFS for each of the plots in Figure 13 (inset map), and was constructed by extrapolating foliation measurements at the surface down to subsurface geophysical images of the indenter front along the transects in Figure 1 (see Schmid & Kissling 2000; TRANSALP Working Group 2002; for summaries of these images). The lines emanating from the periphery of the Ls pole plots show the average foliation trends and the thin black arrows indicate the motion parallel to the stretching lineations. Large, open arrows indicate the inferred, bulk extensional direction, as discussed below.

Most of the pole patterns are very symmetrical and comprise great-circle maxima or point maxima that lie on great circles. In the Eastern Alps, these great circles define cross-girdle patterns and subhorizontal lineation maxima that reflect conjugate, non-coaxial shearing along the sinistral DAV and dextral Mölltal faults (Fig. 13a), and constrictional folding in both the eastern and western parts of the Tauern window (Fig. 13b). Foliation and lineation maxima for the Brenner and Katschberg extensional faults (Fig. 13c) also outline a composite pattern that is nearly orthogonal to the indenter surface. Conjugate or duplex shearing on these faults and folds therefore extended the orogenic crust subparallel to the indenter surface in the Eastern Alps, as indicated by the open arrows in Figures 13a to c. In contrast, the foliation and lineation maxima along the Tonale segment of the PFS in the Central Alps (Fig. 13d) reflect partitioning of strike–slip and dip–slip motions on a single shearing plane subparallel to the indenter surface. The maxima associated with the Forcola and Simplon extensional faults (Fig. 13e) are oblique to the indenter surface, consistent with oblique, NE–SW directed extension during dextral transpression in the Central Alps. At the western end of the PFS, the Insubric mylonites (Fig. 13f) define a broad foliation maxima with two lineation maxima at a high mutual angle. This indicates strong partitioning of NE–SW lateral extension and SE-directed backthrusting, again subparallel to the indenter surface. The core of the Vanzone antiform defines a single-girdle foliation pattern with a point maxima indicative of coaxial stretching oblique to the indenter surface as defined by the front of the Ivrea geophysical body (Fig. 13g).

The pole patterns described above reveal that oblique, NW motion of the southern Alpine indenter in Oligo-Miocene time was accommodated differently along strike of the Alpine orogen: NNE-directed shortening and E–W extension in the Eastern Alps contrasts with NW–SE shortening and NE–SW extension in the Western and Central Alps. A possible explanation is that the southern Alpine indenter was segmented, with separate eastern and western

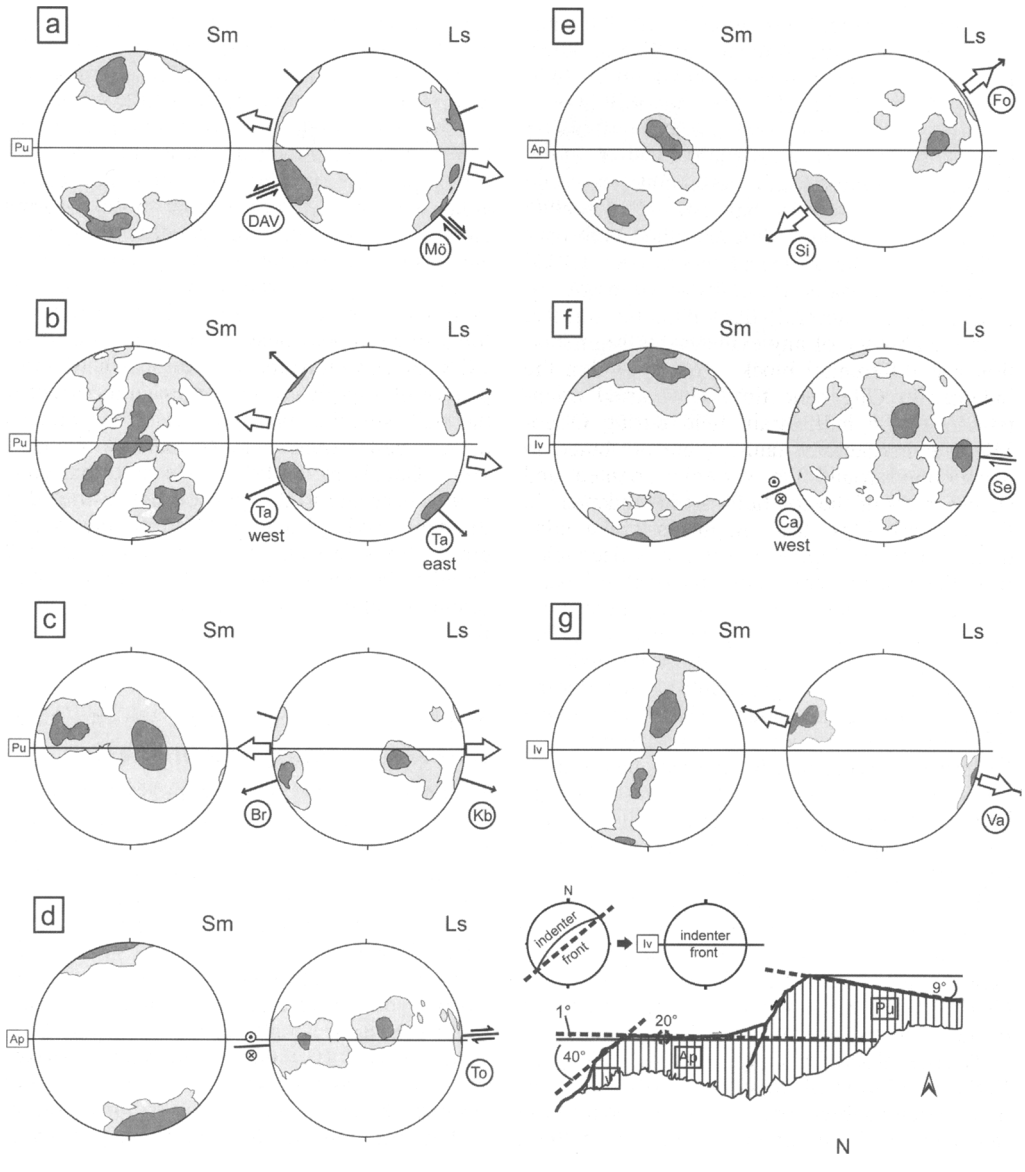


**Fig. 13.** Symmetry and kinematics of mylonitic shearing along the Periadriatic Fault System. Equal area projections contain contoured poles to mylonitic foliation (Sm) and stretching lineation (Ls) with respect to the leading edge of the southern Alpine indenter oriented vertically east–west. Contours in projections taken from Figure 10. (**a**) DAV and Mölltal mylonitic faults and related folds; (**b**) large upright folds in the eastern and western parts of the Tauern window, Eastern Alps; (**c**) Brenner and Katschberg extensional faults, Eastern Alps; (**d**) Tonale segment of the Insubric mylonite belt near the Bergell pluton, Central Alps; (**e**) Forcola and Simplon extensional faults, Central Alps; (**f**) western Canavese segment of the Insubric mylonite belt, Insubric mylonites in the Sesia Zone; (**g**) core of the Vanzone antiform, Western Alps. Angles used for rotating the data in these plots with respect to the indenter surfaces are shown in the lower-right diagram. Boxed abbreviations for the indenter surfaces: Iv, front of Ivrea geopyhsical body; Ap, front of Apulia crustal wedge; Pu, Pustertal fault and its projection to depth. Lines and arrows emanating from Ls pole plots show the average foliation trend and motion sense on the mylonitic fault surfaces. Open arrows indicate bulk extension direction (see text). Abbreviations for fault surfaces as in Figure 1.

blocks rotating clockwise along a mutual boundary defined by the sinistral Giudicarie fault. However, sinistral motion along this fault occurred after 20 Ma (Fig. 11), possibly in conjunction with a reversal of subduction direction beneath the Eastern Alps (Schmid *et al.* 2003, 2004). Furthermore, rigid block rotations within the main edifice of the Alps are only plausible for late middle to late Miocene time (Laubscher 1996) when the orogenic crust had cooled sufficiently to enable rigid, brittle behaviour of basement units currently exposed at the surface.

In the absence of any evidence for segmentation and differential block rotations within the indenter in Oligocene time, the varied orientations of the bulk strain field during Oligo-Miocene Periadriatic faulting are attributed to decoupling around the variably oriented and shaped parts of the southern Alpine indenter. In the Eastern Alps, the straight, northern edge of the southern Alpine indenter was decoupled from the orogenic crust along the dextral Pustertal fault. The lateral, E–W displacement component of oblique convergence was therefore taken up by brittle faulting along the indenter surface, leaving conjugate faulting and folding to accommodate the normal, NNE-displacement component within the exhuming, orogenic crust in front of the indenter. In contrast, the orogenic crust in the Western Alps was constrained to flow up (to the SE) and around (to the NE) the angular, steeply NW-dipping edge of the geophysical Ivrea body (Fig. 12). The exhumational component of shear was concentrated at the indenter surface in the Insubric mylonite belt. Once the crust flowed around this restraining bend, it underwent NE–SW extension in the Central Alps, leading to the Miocene exhumation of the Lepontine thermal dome.

The coeval activity of mylonitic faults along the PFS from 35 to 15 Ma together with the affinity of bulk stretching directions accommodated by these faults to the local orientation of the southern Alpine indenter surface suggest that the leading edge of this indenter was the macroscopic shearing plane for Insubric deformation. Furthermore, the fact that foliation and lineation pole patterns are highly symmetrical and define slip systems that are systematically disposed with respect to the indenter surface support the idea that the pre-existing schistosities rotated into orientations which maximized the component of simple shearing within these slip systems.

The kinematic significance of rotating anisotropies by folding and shearing in a general non-coaxial strain field is therefore that stable or semi-stable orientations of shear zones are attained for which the bulk stretching direction corresponds to an eigenvector of flow, that is, a direction along which the rate of flow is the greatest and toward which all passive markers within a rock tend to rotate. Similar to our analysis above, Cobbold & Gapais (1986) compared networks of outcrop-scale shear zones to ideal fibre-type slip systems in which slip occurs along inextensible lines parallel to the shearing direction. At least three independent slip systems are needed to maintain strain compatibility during bulk plane-strain deformation, and the minimum number of systems increases to five for a three-dimensional strain field (von Mises 1928). Accordingly, the orientational distribution pattern of slip-planes and -lines with respect to the bulk shearing plane reflects the symmetry of the bulk strain field (Gapais & Cobbold 1987; Gapais *et al.* 1987). We note that combined shear-and-fold zones are not restricted to the Alps, having been identified in other deeply eroded transpressional fault zones (e.g. Ebert & Hasui 1998) which appear to have similar fabric orientational distributions as those described for the PFS.

## Significance for crustal strength and force transmission through the lithosphere

Decoupling related to strain partitioning in the viscous continental crust presents an interesting dynamic problem, because intracrustal strain partitioning was previously thought to occur in much shallower levels, at the interface of the viscous crust with the brittle, upper crust (e.g. Richard & Cobbold 1989; Molnar 1992). Molnar (1992) attributed this to the apparent inability of a horizontal viscous layer to transmit shear stresses to an attached brittle layer above. Yet, we have seen that partitioning of strike–slip and dip–slip shearing along the PFS occurred below the brittle-to-viscous transition.

The solution to this discrepancy between Nature and experiment lies with the fact that crustal rocks are mechanically anisotropic, primarily due to the strong mechanical anisotropy of sheet silicates, especially micas in schistose rock. The mechanical effect of rotating a weak, pre-existing anisotropy into parallelism with the shearing plane is two-fold. The resolved shear stress in directions parallel to this anisotropy (i.e. the weak direction) will increase, while the volume proportion of deforming rock that is optimally oriented to maximize simple shear in these directions also increases. Folding or shearing an anisotropic rock therefore weakens it, an effect known in rock mechanics as 'rotation-weakening' (Cobbold 1977) or 'foliation-weakening'

(Jordan 1988). By analogy with experimental and theoretical work on bimineralic aggregates (Handy 1990), the weakening associated with the formation of new faults depends on the volume proportion of mylonitic faults oriented parallel to the shearing plane, and on the relative strength of the fault rocks and the less-deformed country rock. Thus, even small volumes of fault rock suffice to weaken the entire crust significantly (Handy 1994). For example, if the strike–slip faults make up 5–10% of the crustal, and the strength ratio of less-deformed rock to fault rock is taken to be 3:1 (a conservative estimate), then polyphase flow laws predict a strength drop of about 20%. Although greater strength drops are expected for larger strength contrasts, this estimate may be a maximum for energetic reasons (Handy 1994).

The notion that plate-scale fault systems rotate into stable end-orientations to accommodate high shear strain is similar to the 'easy glide' concept first proposed by E. Schmid (1928) to explain the rotation of crystallographic slip systems toward stable orientations of high resolved shear stress during crystal–plastic deformation of polycrystalline aggregates. An important difference, however, is that the potential glide direction (i.e. the Burger's vector) in an intracrystalline slip system is limited by the crystallography and orientation of the host grain in a polycrystalline aggregate (e.g. Taylor 1938), whereas the shearing direction in a mylonitic shear zone is determined primarily by the stress field in the vicinity of the fault array. This local stress field is predictably related to the far-field, plate-scale stress field if the configuration, orientation and length-scale of the fault array have become strain-invariant.

An important implication of the above for plate tectonics is that weakening and intracrustal decoupling in the viscous crust do not preclude the vertical transmission of normal and shear stresses through the lithosphere. Although Molnar's (1992) idea that shear stresses cannot be transmitted upward across horizontal viscous layers is correct if these layers have very low viscosity and are both homogeneous and isotropic, it evidently does not apply to heterogeneous, anisotropic media like folded, foliated basement rocks (Cobbold 1977). Decoupling along and across networked folds and mylonitic faults in the viscous continental crust ensures that deformation between the stronger subcontinental mantle and overlying brittle crust remains compatible, even at high shear strains where the incompatibility in strain between these layers with disparate strengths is potentially very large. The increased volume proportion of weak, folded and sheared rock in the viscous crust decreases the bulk, horizontal shear strength of the viscous crust, and therefore also of the lithosphere. Yet, the strain-dependent rotation of weak anisotropies towards the macroscopic shearing plane also increases the volume proportion of weak rock oriented at high angles to the greatest principal stress direction. Thus, the plate forces transmitted across an intracrustal decoupling zone are inferred to remain constant or even to increase at constant bulk strain rate. The same principle of strain-dependent, strength reduction at constant or even increasing plate-scale force may also apply to relatively weak, decoupling layers in the mantle. To speak of the continental crust beneath the brittle–viscous transition as a horizontal 'attachment zone' (Tikoff *et al.* 2002) is misleading, because the vertical transmission of plate forces that potentially facilitates strike–slip faulting along plate boundaries in the upper crust (e.g. Li & Rice 1987) may also involve detachment of the upper crust from the upper mantle, that is, decoupling in the sense defined at the outset of this paper. Therefore, a more appropriate term for a weak, heterogeneously sheared, anisotropic layer that transmits stress through the lithosphere is 'accommodation zone'.

## A generic model of decoupling and strain partitioning

The block diagram in Figure 14 is a generic model of intracrustal decoupling in orogenic crust based on the Periadriatic fault system. Decoupling is concentrated along the leading edge of the orogenic indenter, where faulting initiates along pre-existing lithological boundaries, in this case between the Early Mesozoic, rifted margin of the southern Alps and the previously subducted and exhumed nappes in the retro-wedge of the Tertiary Alpine orogen. The rheological contrast at the indenter surface is accentuated by lateral thermal gradients during mylonitic thrusting of the hot, orogenic retro-wedge onto the cold indenter. Decreasing temperature in the retro-wedge enhances strain localization and increases the strain rate, leading to viscous instabilities and the generation of pseudotachylite near the indenter surface. Within the warm retro-wedge of the orogen, older foliations are folded and steepen to form subvertical mylonitic faults and constrictional folds that accommodate stretching parallel to subparallel to the indenter surface. The steep mylonitic faults are potential conduits for the rapid ascent of mantle-derived melts, some of

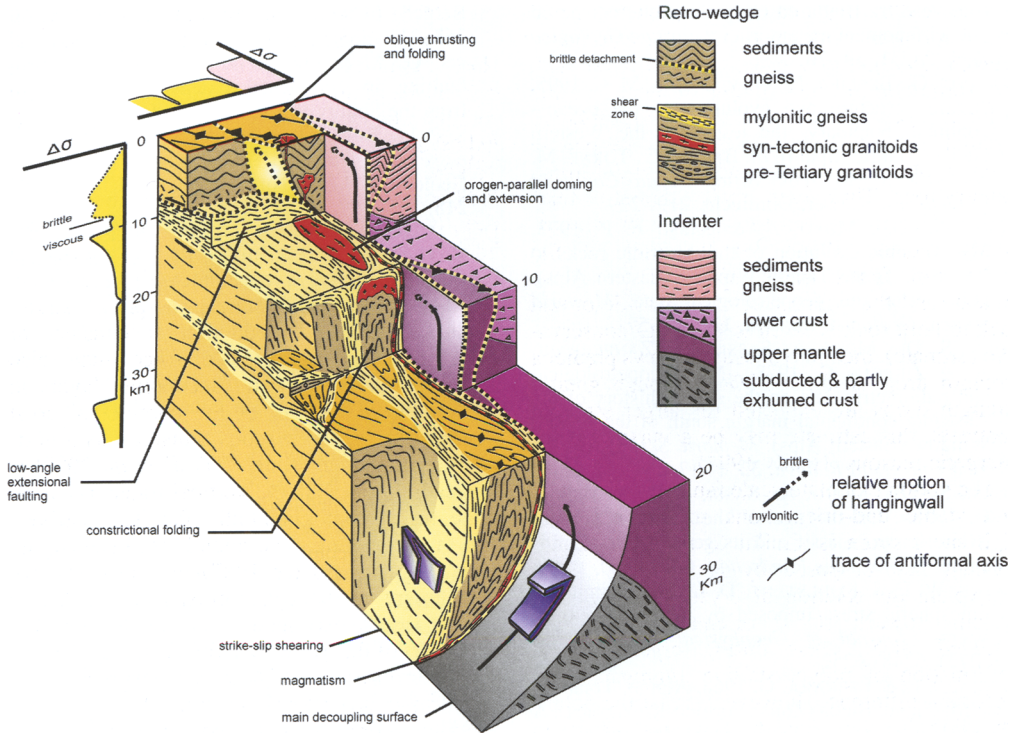


**Fig. 14.** Generic model of decoupling zones related to strain partitioning along the Periadriatic fault system.

which (like the Rieserferner and Bergell plutons) are emplaced in the cores of antiforms below the brittle-to-viscous transition. These mylonitic faults are optimally oriented to accommodate simple shearing and are predicted to weaken the orogenic crust by up to 20%. Further away from the indenter and/or in shallower crustal levels, orogen-parallel extension is accommodated by low-angle normal faults, which detach the exhuming ductile crust from the brittle, upper crust.

We have shown that complex patterns of folding and faulting during transpressional deformation in orogenic crust can be interpreted in terms of decoupling in different crustal levels. The future characterization of such structures in other deeply eroded, ancient fault systems may help us to understand how stress and strain are transferred across active continental fault systems.

We thank the reviewers, D. Marquer and L. Ratschbacher, for helpful comments, and our colleagues (K. Hammerschmidt, R. Oberhänsli, G. Gosso, I. Spalla, M. Zucali, R. Bousquet, S. M. Schmid, H. Stünitz) for spirited discussions. This work was facilitated by the mapping of several Diploma students in parts of the areas described above: M. Albertz, J. Giese, R. Häusler, M. Janitschke, S. Lüdtke, C. Möbus, I. Schindelwig and B. Sperber. Our work was financed largely by the Deutsche Forschungs Gemeinschaft (DFG) in the form of two 2.5-year grants (Ha 2403/3, Ha 2403/5) and by one-year assistantships to J.B., M.K. and R.W. from the Freie Universität Berlin.

## References

ARGAND, E. 1916. Sur l'arc des Alpes Occidentales. *Eclogae geologicae Helvetiae*, **14**, 145–191.

AXEN, G. J., SELVERSTONE, J. & WAWRZYNIEC, T. 2001. High-temperature embrittlement of extensional Alpine mylonite zones in the mid-crustal ductile–brittle transition. *Journal of Geophysics*, **106**, 437–448.

BEHRMANN, J. H. 1988. Crustal-scale extension in a convergent orogen. The Sterzing–Steinach mylonite zone in the Eastern Alps. *Geodynamica Acta*, **2**, 63–73.

BERGER, A., ROSENBERG, C. & SCHMID, S. M. 1996. Ascent, emplacement and exhumation of the Bergell pluton within the Southern Steep Belt of the Central Alps. *Schweizerische Mineralogische und Petrographische Mitteilungen*, **76**, 357–382.

BIANCHI, A. & DAL PIAZ, G. V. 1963. Gli inclusi di 'micaschisti eclogitici' della zona Sesia nella formazione porfiritica permiana della zone del

Canavese fra Biella ed Oropa; charatteristiche ed eta dei fenomeni metamorfici. *Giornale Geologico Serie 2a*, **31**, 39–76.

BOILLOT, G., BESLIER, M. O. & COMAS, M. C. 1995. Nature, structure and evolution of the ocean–continent boundary: the lesson of the Western Galicia Margin (Spain). *In*: BANDA, E., TORNÉ, M. & TALWANI, M. (eds) *Rifted Ocean–Continent Boundaries.* Kluwer, Dordrecht, 219–229.

BORSI, S., DEL MORO, A. & SASSI, F. P. 1973. Metamorphic evolution of the Austridic rocks to the south of the Tauern Window (Eastern Alps): radiometric and geopetrological data. *Memoria Società Geologica Italiana*, **12**, 549–571.

BORSI, S., DEL MORO, A., SASSI, F. P., ZANFERRARI, A. & ZIRPOLI, G. 1978*a*. New geopetrological and radiometric data on the Alpine history of the Austridic continental margin south of the Tauern Window (Eastern Alps). *Memorie Scienze Geologica Università Padova*, **32**, 1–17.

BORSI, S., DEL MORO, A., SASSI, F. P. & ZIRPOLI, G. 1978*b*. On the age of the Vedrette di Ries (Rieserferner) massif and its geodynamic significance. *Geologische Rundschau*, **68**, 41–60.

BRACE, W. F. & KOHLSTEDT, D. L. 1980. Limits on lithospheric stress imposed by laboratory experiments. *Journal of Geophysical Research*, **85** (B11), 6248–6252.

CARRARO, F. & FERRARA, G. 1968. Alpine 'Tonalite' at Magliano, Biella (Zona Dioritico-Kinzigitica). A preliminary note. *Schweizerische Mineralogische und Petrographische Mitteilungen*, **48**, 75–80.

CESARE, B. 1992. Metamorfismo di contatto di rocce pelitiche nell' aureola di Vedrette di Ries (Alpi Orientali Italia). *Atti Ticinensi di Scienze della Terra*, **35**, 1–7.

CESARE, B. 1994. Hercynite as a product of staurolite decomposition in the contact aureole of Vedrette di Ries, eastern Alps, Italy. *Contributions to Mineralogy and Petrology*, **116**, 239–246.

CHESTER, F. M. 1995. A rheologic model for wet crust applied to strike–slip faults. *Journal of Geophysical Research*, **100** (B7), 13033–13044.

CLIFF, R. A., DROOP, G. T. R. & REX, D. C. 1985. Alpine metamorphism in the south-east Tauern Window, Austria: 2. Rates of heating, cooling and uplift. *Journal of Metamorphic Geology*, **3**, 403–415.

CLIFF, R. A., NORRIS, R. J., OXBURGH, E. R. & WRIGHT, R. C. 1971. Structural, metamorphic and geochronological studies in the Riesseck and Southern Ankogel Groups, the Eastern Alps. *Jahrbuch des Geologischen Bundesanstalts Wien*, **114**, 121–272.

COBBOLD, P. R. 1977. Description and origin of banded deformation structures. II. Rheology and the growth of banded perturbations. *Canadian Journal of Earth Sciences*, **14**, 2510–2523.

COBBOLD, P. R. & GAPAIS, D. 1986. Slip-system domains. I. Plane-strain kinematics of arrays of coherent bands with twinned fibre orientations. *Tectonophysics*, **131**, 113–132.

DAVIDSON, C., ROSENBERG, C. & SCHMID, S. M. 1996. Synmagmatic folding of the base of the Bergell pluton, Central Alps. *Tectonophysics*, **265**, 213–238.

DAVIS, G. A. & LISTER G. S. 1988. Detachment faulting in continental extension: perspectives from the Southwestern US Cordillera. *In*: CLARK, S. P. JR., BURCHFIEL, B. C. & SUPPE J. (eds) *Processes in Continental Lithospheric Deformation.* Geological Society of America, Special Papers, **218**, 133–159.

DEL MORO, A., PARDINI, G. C., QUERCIOLI, C., VILLA, I. M. & CALLEGARI, E. 1983. Rb/Sr and K/Ar chronology of Adamello granitoids, southern Alps. *Memorie della Società Geologica Italiana*, **26**, 285–299.

DERCOURT, J., ZONENSHAIN, L. P. *et al.* 1986. Geological evolution of the Tethys belt from the Atlantic to the Pamirs since the Lias. *Tectonophysics*, **123**, 241–315.

DEWEY, J. F., HELMAN, M. L., TURCO, E., HUTTON, D. H. W. & KNOTT, S. D. 1989. Kinematics of the Western Mediterranean. *In*: COWARD, M. P., DIETRICH, D. & PARK, R. G. (eds) *Alpine Tectonics.* Geological Society, London, Special Publications, **45**, 265–283.

DUCHÊNE, S., BLICHERT-TOFT, J., LUAIS, B., TÉLOUK, P., LARDEAUX, J.-M. & ALBARÈDE, F. 1997. The Lu-Hf dating of garnets and the ages of the Alpine high-pressure metamorphism. *Nature*, **387**, 586–588.

DUNKL, I., FRISCH, W. & GRUNDMANN G. 2003. Zircon fission track thermochronology of the southeastern part of the Tauern Window and the adjacent Austroalpine margin, Eastern Alps. *Eclogae geologicae Helvetiae*, **96**, 209–217.

EBERT, H. D. & HASUI, Y. 1998. Transpressional tectonics and strain partitioning during oblique collision between three plates in the Precambian of southeast Brazil. *In*: HOLDSWORTH, R. E., STRACHAN, R. A. & DEWEY, J. F. (eds) *Continental Transpressional and Transtensional Tectonics.* Geological Society, London, Special Publications, **135**, 231–252.

ESCHER, A. & BEAUMONT, C. 1997. Formation, burial and exhumation of basement nappes at crustal scale: a geometric model based on the Western Swiss–Italian Alps. *Journal of Structural Geology*, **19** (7), 955–974.

FISCH, H. R. 1989. Zur Kinematik der südlichen Steilzone der Zentralalpen, E von Bellinzona. *Schweizerische Mineralogische und Petrographische Mitteilungen*, **69**, 377–393.

FOSSEN, H. & TIKOFF, B. 1998. Extended models of transpression and transtension, and application to tectonic settings. *In*: HOLDSWORTH, R. E., STRACHAN, R. A. & DEWEY, J. F. (eds) *Continental Transpressional and Transtensional Tectonics.* Geological Society, London, Special Publications, **135**, 15–33.

FRISCH, W., KUHLEMANN, J., DUNKL, I. & BRÜGEL, A. 1998. Palinspastic reconstruction and topographic evolution of the Eastern Alps during late Tertiary tectonic extrusion. *Tectonophysics*, **297**, 1–15.

FRISCH, W., DUNKL, I. & KUHLEMANN, J. 2000. Post-collisional orogen-parallel large-scale extension in the Eastern Alps. *Tectonophysics*, **327**, 239–265.

FROITZHEIM, N., SCHMID, S. M. & FREY, M. 1996. Mesozoic paleogeography and the timing of eclogite-facies metamorphism in the Alps: a working hypothesis. *Eclogae geologicae Helvetiae*, **89** (1), 81–110.

FÜGENSCHUH, B., SEWARD, D. & MANCKTELOW, N. 1997. Exhumation in a convergent orogen: the western Tauern window. *Terra Nova*, **9**, 213–217.

GAPAIS, D. & COBBOLD, P. R. 1987. Slip system domains. 2. Kinematic aspects of fabric development in polycrystalline aggregates. *Tectonophysics*, **138**, 289–309.

GAPAIS, D., BALE, P., CHOUKROUNE, P., COBBOLD, P. R., MAHJOUB, Y. & MARQUER, D. 1987. Bulk kinematics from shear zone patterns: Some field examples. *Journal of Structural Geology*, **9** (5/6), 635–646.

GENSER, J. & NEUBAUER, F. 1989. Low-angle normal faults at the eastern margin of the Tauern window (Eastern Alps). *Mitteilungen der Österreichischen Geologischen Gesellschaft*, **81**, 233–243.

GIGER, M. & HURFORD, A. J. 1989. Tertiary intrusives of the Central Alps: Their Tertiary uplift, erosion, redeposition and burial in the south Alpine foreland. *Eclogae geologicae Helvetiae*, **82**, 857–866.

GOSSO, G., DAL PIAZ, G. V., PIOVANO, V. & POLINO, R. 1979. High pressure emplacement of early-Alpine Nappes, post-nappe deformations and structural levels (internal northwestern Alps). *Memorie Istituto di Mineralogia e Petrografia dell' Università di Padova*, **32**, 5–15.

GRASEMANN, B. & MANCKTELOW, N. 1993. Two-dimensional thermal modelling of normal faulting: the Simplon Fault Zone, Central Alps, Switzerland. *Tectonophysics*, **225**, 155–165.

GUNZENHAUSER, B. 1985. Zur Sedimentologie und Paläogeographie der oligo-miocaenen Gonfolite Lombarda zwischen Lago Maggiore und der Brianza (Südtessin, Lombardei). *Beiträge zur geologischen Karte der Schweiz*, NF, **159**.

HANDY, M. R. 1990. The solid-state flow of polymineralic rocks. *Journal of Geophysical Research*, **96** (B6), 8647–8661.

HANDY, M. R. 1994. The energetics of steady state heterogeneous shear in mylonitic rock. *Materials Science and Engineering*, **A175**, 261–272.

HANDY, M. R. & ZINGG, A. 1991. The tectonic and rheologic evolution of an attenuated cross section of the continental crust: Ivrea crustal section, southern Alps, northwestern Italy and southern Switzerland. *Geological Society of America Bulletin*, **103**, 236–253.

HANDY, M. R. & OBERHÄNSLI, R. 2004. Metamorphic structure of the Alps: tectonometamorphic age map. *In*: OBERHÄNSLI, R. (ed) *Explanatory Notes to the Map of Metamorphic Structures of the Alps*. Mitteilungen der Österreichischen Mineralogischen Gesellschaft, **49**, 201–226.

HARLAND, W. B., ARMSTRONG, A. V., COX, L. E., CRAIG, A. G. & SMITH, D. G. 1989. *A Geologic Time Scale*. Cambridge University Press, New York.

HOBBS, B. E., ORD, A. & TEYSSIER, C. 1986. Earthquakes in the ductile regime? *Pure and Applied Geophysics*, **124** (1/2), 309–336.

HOINKES, G., KOLLER, F., RANTITSCH, D., DACHS, E., HÖCK, V., NEUBAUER, F. & SCHUSTER, R. 1999. Alpine metamorphism of the Eastern Alps. *Schweizerische Mineralogische und Petrographische Mitteilungen*, **79** (1), 155–182.

HOLT, W. E. 2000. Correlated crust and mantle strain fields in Tibet. *Geology*, **28** (1), 67–70.

HUNZIKER, J. C. 1974. Rb-Sr and K-Ar age determinations and the Alpine tectonic history of the Western Alps. *Memorie Geologica della Università di Padova*, **31**, 1–54.

HUNZIKER, J. C., DESMONS, J. & HURFORD, A. J. 1992. Thirty-two years of geochronological work in the Central and Western Alps: a review on seven maps. *Mémoires de Géologie (Lausanne)*, **13**, 1–59.

HURFORD, A. J. 1986. Cooling and uplift patterns in the Lepontine Alps, South Central Switzerland and an age of vertical movement on the Insubric fault line. *Contributions to Mineralogy and Petrology*, **92**, 413–427.

HURFORD, A. J., HUNZIKER, J. C. & STÖCKERT, B. 1991. Constraints on the late thermotectonic evolution of the western Alps: Evidence for episodic rapid uplift. *Tectonics*, **10** (4), 758–769.

INGER, S. & CLIFF, R. A. 1994. Timing of metamorphism in the Tauern Window, Eastern Alps: Rb-Sr ages and fabric formation. *Journal of Metamorphic Geology*, **12**, 695–707.

INGER, S., RAMSBOTHAM, W., CLIFF, R. A. & REX, D. C. 1996. Metamorphic evolution of the Sesia Lanzo Zone, Western Alps: time constraints from multi-system geochronology. *Contributions to Mineralogy and Petrology*, **126**, 152–168.

JORDAN, P. 1988. The rheology of polymineralic rocks – an approach. *Geologische Rundschau*, **77** (1), 285–294.

KLEINSCHRODT, R. 1987. Quarzkorngefügeanalyse im Altkristallin südlich des westlichen Tauernfensters (Südtirol/Italien). *Erlanger Geologische Abhandlungen*, **114**, 1–82.

KURZ, W. & NEUBAUER, F. 1996. Deformation partitioning during updoming of the Sonnblick area in the Tauern Window (Eastern Alps, Austria). *Journal of Structural Geology*, **18** (11), 1327–1343.

LACASSIN, R. 1989. Plate scale kinematics and compatibility of crustal shear zones in the Alps. *In*: COWARD, M. P., DIETRICH, D., PARK, R. (eds) *Alpine Tectonics*. Geological Society, London, Special Publications, **45**, 339–352.

LAMMERER, B. & WEGER, M. 1996. Footwall uplift in an orogenic wedge: the Tauern Window in the Eastern Alps of Europe. *Tectonophysics*, **285**, 213–230.

LAUBSCHER, H. 1991. The arc of the Western Alps today. *Eclogae Geologica Helvetiae*, **84** (3), 631–659.

LAUBSCHER, H. 1996. Shallow and deep rotations in the Miocene Alps. *Tectonics*, **15**, 1022–1035.

LI, V. C. & RICE, J. R. 1987. Crustal deformation in Great California earthquake cycles. *Journal of Geophysical Research*, **92** (B11), 11533–11551.

MADDOCK, R. 1983. Melt orogin of pseudotachylites demonstrated by textures. *Geology*, **11**, 105–108.

MAGLOUGHLIN, J. F. & SPRAY, J. G. 1992. Frictional melting processes and products in geological materials: introduction and discussion. *Tectonophysics*, **204**, 197–204.

MANCKTELOW, N. S. 1990. The Simplon Fault Zone. *Beiträge zur Geologie der Schweiz*, **163** (Neue Folge), 1–74.

MANCKTELOW, N. S. 1992. Neogene lateral extension during convergence in the Central Alps: evidence from interrelated faulting and backfolding around the Simplonpass (Switzerland). *Tectonophysics*, **215**, 295–317.

MANCKTELOW, N. S., STÖCKLI, D. F. *et al.* 2001. The DAV and Periadriatic fault systems in the Eastern Alps south of the Tauern window. *In*: FRISCH, W. & MANCKTELOW, N. S. (eds) *Developments in Alpine Geodynamics. International Journal of Earth Sciences*, Springer, Berlin, **90** (3), 593–622.

MCNULTY, B. A. 1995. Peudotachylyte generated in the semi-brittle and brittle regimes, Bench Canyon shear zone, central Sierra Nevada. *Journal of Structural Geology*, **17** (11), 1507–1521.

MEANS, W. D. 1989. Stretching faults. *Geology*, **17**, 893–896.

MEYRE, C., MARQUER, D., SCHMID, S. M. & CIANCALEONI, L. 1998. Syn-orogenic extension along the Forcola fault: Correlation of Alpine deformations in the Tambo and Adula nappes (Eastern Penninic Alps). *Eclogae Geologicae Helvetiae*, **91**, 409–420.

MILNES, G. 1974. Structure of the pennine zone (central Alps): A new working hypothesis. *Geological Society of America Bulletin*, **85**, 1725–1732.

MOONEY, W. D. & GINZBURG, A. 1986. Seismic measurements of the internal properties of fault zones. *Pure and Applied Geophysics*, **124** (1/2), 141–157.

MOLNAR, P. 1992. Brace-Goetze strength profiles, the partitioning of strike–slip and thrust faulting at zones of oblique convergence, and the stress–heat flow paradox of the San Andreas Fault. *In*: EVANS, B. & WONG, T. F. (eds) *Fault Mechanics and Transport Properties of Rocks: A Festschrift in Honor of W. F. Brace.* International Geophysics Series, **51**, 435–460.

MOST, P. 2003. *Late Alpine cooling histories of tectonic blocks along the central part of the TRANSALP traverse (Inntal-Gardatal): constraints from geochronology.* PhD thesis, Universität Tübingen.

MÜLLER, W., MANCKTELOW N. S. & MEIER, M. (2000) Rb–Sr microchrons of synkinematic mica in mylonites: an example from the DAV fault of the Eastern Alps. *Earth and Planetary Science Letters*, **180**, 385–397.

MÜLLER, W., PROSSER, G., MANCKTELOW, N. S., VILLA, I. M., KELLEY, S. P., VIOLA, G. & OBERLI, F. 2001. Geochronological constraints on the evolution of the Periadriatic Fault System (Alps). *In*: FRISCH, W. & MANCKTELOW, N. S. (eds) *Developments in Alpine Geodynamics. International Journal of Earth Sciences*, Springer, Berlin, **90** (3), 623–653.

NICOLAS, A., POLINO, R., HIRN, A., NICOLICH, R. & the Ecors-Crop working group. 1991. Ecors-Crop traverse and deep structure of the western Alps. A synthesis. *In*: ROURE, F., HEITZMANN, P. & POLINO, R. (eds) *Deep Structure of the Alps.* Mémoire Société Géologique de France, Paris, **156**; Mémoire Société Géologique de Suisse, Zürich, **1**; Volume speciale de Società Geologica Italiana, Roma, **1**, 15–28.

NIEVERGELT, P., LINIGER, M., FROITZHEIM, N. & FERREIRO MÄHLMANN, R. 1996. Early to mid Tertiary crustal extension in the Central Alps: The Turba Mylonite Zone (Eastern Switzerland). *Tectonics*, **15** (2), 329–340.

OBERLI, F., MEIER, M., BERGER, A., ROSENBERG, C. & GIERÉ, R. 2004. U–Th–Pb and 230Th/238U disequilibrium isotope systematics: precise accessory mineral chronology and melt evolution tracing in the Alpine Bergell Intrusion. *Geochimica et Cosmochimica Acta*, **68**, 2543–2560.

OLIVER, G. J. H. & COGGON, J. H. 1979. Crustal structure of Fiordland, New Zealand. *Tectonophysics*, **54**, 253–292.

PIERI, M. & GROPPI, G. 1981. Subsurface geological structure of the Po Plain, Italy. Progettto Finalizzato Geodinamica, *CNR Publication*, **414**, 113–321, Rome, Italy.

POLINSKI, R. K. & EISBACHER, G. H. 1991. Deformation partitioning during polyphase oblique convergence in the Karawanken Mountains, southeastern Alps. *Journal of Structural Geology*, **14** (10), 1203–1213.

PROSSER, G. 1998. Strike–slip movements and thrusting along a transpressive fault zone: the Northern Giudicarie line (Insubric line, northern Italy). *Tectonics*, **17**, 921–937.

RANALLI, G. & MURPHY, D. C. 1987. Rheological stratification of the lithosphere. *Tectonophysics*, **132** (4), 281–296.

RATSCHBACHER, L., MERLE, O., DAVY, P. & COBBOLD, P. 1991*a*. Lateral extrusion in the eastern Alps, Part 1: boundary conditions and experiments scaled for gravity. *Tectonics*, **10** (2), 245–256.

RATSCHBACHER, L., FRISCH, W., LINZER, H. G. & MERLE, O. 1991*b*. Lateral extrusion in the eastern Alps, Part 2: structural analysis. *Tectonics*, **10** (2), 257–271.

REDDY, S. M., CLIFF, R. A. & EAST, R. 1993. Thermal history of the Sonnblick Dome, south-east Tauern Window, Austria: implications for heterogeneous uplift within the Pennine basement. *Geologische Rundschau*, **82**, 667–675.

REDDY, S. M., KELLY, S. P. & WHEELER, J. 1996. A 40Ar/39Ar laser probe study of micas from the Sesia Zone, Italian Alps: implications for metamorphic and deformation histories. *Journal of Metamorphic Geology*, **14**, 493–508.

REDDY, S. M., WHEELER, J. & CLIFF, R. A. 1999. The geometry and timing of orogenic extension: an

example from the Western Italian Alps. *Journal of Metamorphic Geology*, **17**, 573–589.

REDDY, S. M., WHEELER, J. *et al.* 2003. Kinematic reworking and exhumation within the convergent Alpine Orogen. *Tectonophysics*, **365**, 77–102.

REINHARDT, B. 1966. Geologie und Petrographie der Monte-Rosa Zone, der Sesia Zone und des Canavese im Gebiet zwischen Valle d'Ossola und Val Loana (Prov. di Novara, Italien). *Schweizerische Mineralogische und Petrographische Mitteilungen*, **46** (2), 553–678.

RICHARD, P. & COBBOLD, P. R. 1989. Structures en fleurs positives et décrochements crustaux: modélisation analogique et interprétation mécanique. *Comptes Rendus Académie des Sciences, Paris* Série II, **308**, 553–560.

ROMER, R. L., SCHÄRER, U. & STECK, A. 1996. Alpine and pre-Alpine magmatism in the root-zone of the western Central Alps. *Contributions to Mineralogy and Petrology*, **123**, 138–158.

ROSENBERG, C. L. 2004. Shear zones and magma ascent: A model based on a review of the Tertiary magmatism in the Alps. *Tectonics*, **23**, TC3002, doi:10.1029/2003TC001526.

ROSENBERG, C., BERGER, A. & SCHMID, S. M. 1995. Observations from the floor of a granitoid pluton: Inferences on the driving force of final emplacement. *Geology*, **23** (5), 443–446.

ROYDEN, L. & BURCHFIEL, B. C. 1989. Are systematic variations in thrust belt style related to plate boundary processes? (The western Alps versus the Carpathians). *Tectonics*, **8** (1), 51–61.

RUBATTO, D., GEBAUER, D. & COMPAGNONI, R. 1999. Dating of eclogite-facies zircons: the age of Alpine metamorphism in the Sesia-Lanzo Zone (Western Alps). *Earth and Planetary Science Letters*, **167**, 141–158.

RUFFET, G., GRUAU, G., BALLÈVRE, M., FÉRAUD, G. & PHILLIPOT, P. 1997. Rb–Sr and 40Ar–39Ar laser probe dating of high-pressure phengites from the Sesia Zone (Western Alps): underscoring of excess argon and new age constraints on the high-pressure metamorphism. *Chemical Geology*, **141**, 1–18.

SCHARBART, S. 1975. Radiometrische Altersdaten von Intrusivgesteinen im Raum Eisenkappel (Karawanken, Kärnten). *Verhandlungen der Geologischen Bundesanstalt, Wien*, **4**, 301–304.

SCHÄRER, U., COSCA, M., STECK, A. & HUNZIKER, J. C. 1996. Termination of major ductile strike–slip shear and differential cooling along the Insubric line (Central Alps): U–Pb, Rb–Sr and 40Ar/39Ar ages of cross-cutting pegmatites. *Earth and Planetary Science Letters*, **142**, 331–351.

SCHMID, E. 1928. Zn-normal stress law. In: *Proceedings of the International Congress on Applied Mechanics*, Delft.

SCHMID, S. M. & HANDY, M. R. 1991. Towards a genetic classification of fault rocks: geological usage and tectonophysical implications. *In*: HSÜ, K. J., MACKENZIE, J. & MÜLLER, D. (eds) *Controversies in Modern Geology*. Academic Press, London, 339–361.

SCHMID, S. M., ZINGG, A. & HANDY, M. R. 1987. The kinematics of movements along the Insubric Line and the emplacement of the Ivrea Zone. *Tectonophysics*, **135**, 47–66.

SCHMID, S. M., AEBLI, H. R., HELLER, F. & ZINGG, A. 1989. The role of the Periadriatic Line in the tectonic evolution of the Alps. *In*: COWARD, M. P., DIETRICH, D. & PARK, R. (eds) *Alpine Tectonics*. Geological Society, London, Special Publications, **45**, 153–171.

SCHMID, S. M., PFIFFNER, O. A., FROITZHEIM, N., SCHÖNBORN, G. & KISSLING, E. 1996. Geophysical-geological transect and tectonic evolution of the Swiss-Italian Alps. *Tectonics*, **15** (5), 1036–1064.

SCHMID, S. M. & KISSLING, E. 2000. The arc of the western Alps in the light of geophysical data on deep crustal structure. *Tectonics*, **19** (1), 62–85.

SCHMID, S. M., FÜGENSCHUH, B. & LIPPITSCH, R. 2003: The Western Alps–Eastern Alps transition: tectonics and deep structure. Extended Abstracts TRANSALP conference, Trieste. *Memorie di Scienze Geologische*, **54**, 257–260.

SCHMID, S. M., FÜGENSCHUH, B., KISSLING, E. & SCHUSTER, R. 2004. TRANSMED Transects IV, V and VI: Three lithospheric transects across the Alps and their forelands. *In*: CAVAZZA, W., ROURE, F., SPAKMAN, W., STAMPFLI, G. M. & ZIEGLER, P. A. (eds) *The TRANSMED Atlas: the Mediterranean Region from Crust to Mantle*. Springer Verlag, Berlin.

SCHMID, S. M., FÜGENSCHUH, B., KISSLING, E. & SCHUSTER, R. 2004. Tectonic map and overall structure of the Alpine orogen. *Eclogae Geologicae Helvetiae*, **97**, 93–117.

SCHOLZ, C. H. 1990. *The Mechanics of Earthquakes and Faulting*. Cambridge University Press, Cambridge.

SCHÖNBORN, G. 1999. Balancing cross sections with kinematic constraints: the Dolomites (northern Italy). *Tectonics*, **18**, 527–545.

SELVERSTONE, J. 1988. Evidence for East–West crustal extension in the eastern Alps: implications for the unroofing history of the Tauern Window. *Tectonics*, **7**, 87–105.

SENARCLENS-GRANCY, W. 1965. Zur Grundgebirgs- und Quartärgeologie der Deferegger Alpen und ihrer Umgebung. *Verhandlungen der Geologischen Bundesanstalt*, Sonderheft **G**, 246–255.

SIBSON, R. H. 1975. Generation of pseudotachylite by ancient seismic faulting. *Geophysical Journal of the Royal Astronomical Society*, **43**, 775–784.

SIBSON, R. H. 1977. Fault rocks and fault mechanisms. *Journal of the Geological Society, London*, **133**, 191–213.

STECK, A. & HUNZIKER, J. 1994. The tertiary structural and thermal evolution of the Central Alps – compressional and extensional structures in an orogenic belt. *Tectonophysics*, **238**, 229–254.

STEENKEN, A., SIEGESMUND, S. & HEINRICHS, T. 2002. The emplacement of the Rieserferner Pluton (Eastern Alps, Tyrol): constraints from field observations, magnetic fabrics and microstructures. *Journal of Structural Geology*, **22**, 1855–1873.

STIPP, M., FÜGENSCHUH, B., GROMET, L. P., STÜNITZ, H. & SCHMID, S. M. 2004. Contemporaneous plutonism and strike–slip faulting along the easternmost segment of the Insubric line: the Tonale fault zone north of the Adamello pluton (Italian Alps). *Tectonics*, **23**, doi: 10.1029/2003TC001515.

STÖCKHERT, B. 1984. K–Ar determinations on muscovites and phengites from deformed pegmatites, and the minimum age of Old Alpine deformation in the Austridic basement to the South of the western Tauern Window (Ahrn valley, Southern Tyrol, Eastern Alps). *Neues Jahrbuch der Mineralogie, Abhandlungen*, **150** (2), 103–120.

STÖCKHERT, B., BRIX, M. R., KLEINSCHRODT, R., HURFORD, A. J. & WIRTH, R. 1999. Thermochronometry and microstructures of quartz – a comparison with experimental flow laws and predictions on the temperature of the brittle–plastic transition. *Journal of Structural Geology*, **21**, 351–369.

SYLVESTER, A. G. 1988. Strike–slip faults. *Geological Society of America Bulletin*, **100**, 1666–1703.

TAYLOR, G. I. 1938. Plastic strain in metals. *Journal of the Institute of Metals*, **62**, 307–324.

TEYSSIER, C. & TIKOFF, B. 1998. Strike–slip partitioned transpression of the San Andreas fault system: a lithospheric-scale approach. *In*: HOLDSWORTH, R. E., STRACHAN, R. A. & DEWEY, J. F. (eds) *Continental Transpressional and Transtensional Tectonics*. Geological Society, London, Special Publications, **135**, 143–158.

TEYSSIER, CH., TIKOFF, B. & WEBER, J. 2002. *Attachment Between Brittle and Ductile Crust at Wrenching Plate Boundaries*. EGS Stephan Mueller Special Publication Series, **1**, 119–144.

TIKOFF, B., TEYSSIER, CH. & WATERS, CH. 2002. *Clutch Tectonics and the Partial Attachment of Lithospheric Layers*. EGU Stephan Mueller Special Publication Series, **1**, 57–73.

TRANSALP Working Group. 2002. First deep seismic reflection images of the Eastern Alps reveal giant crustal wedges and transcrustal ramps. *Geophysical Research Letters*, **29** (10), 1029/2002GL014911.

TSE, S. T. & RICE, J. R. 1986. Crustal earthquake instability in relation to the depth variation of frictional slip properties. *Journal of Geophysical Research*, **91** (B9), 9452–9472.

VALASEK, P. & MÜLLER, ST. 1997. A 3D crustal model of the Swiss Alps based on an integrated interpretation of seismic refraction and NRP 20 seismic reflection data. *In*: PFIFFNER, O. A., LEHNER, P., HEITZMANN, P., MUELLER, ST. & STECK, A. (eds) *Results of NRP 20: Deep Structure of the Swiss Alps*. Birkhäuser Verlag, Basel, Boston, Berlin, 305–325.

VAUCHEZ, A. & TOMMASI, A. 2003. Wrench faults down to the asthenosphere: geological and geophysical evidence and thermo-mechanical effects. *In*: STORTI, F., HOLDSWORTH, R. E. & SALVANI, F. (eds) *Intraplate Strike–Slip Deformation Belts*. Geological Society, London, Special Publications, **210**, 15–34.

VILLA, I. & VON BLANCKENBURG, F. 1992. A hornblende Ar–Ar age traverse of the Bregaglia tonalite (SE Central Alps). *Schweizerische Mineralogische und Petrographische Mitteilungen*, **71**, 73–87.

VIOLA, G., MANCKTELOW, N. & SEWARD, D. 2001. Late Oligocene evolution of Europe–Adria collision: New structural and geochronological evidence from the Giudicarie fault system (Italian Eastern Alps). *Tectonics*, **20** (6), 999–1020.

VON BLANCKENBURG, F., VILLA, I. M., BAUER, H., MORTEANI, G. & STEIGER, R. H. 1989. Time calibration of a PT-path from the Western Tauern Window, Eastern Alps: the problem of closure temperatures. *Contributions to Mineralogy and Petrology*, **101**, 1–11.

VON MISES, R. 1928. Mechanik der plastischen Formänderung von Kristallen. *Zeitschrift für angewandte Mathematik und Mechanik*, **8**, 161–184.

WAGNER, G. A., MILLER, D. S. & JÄGER, E. 1977. Fission track ages on apatite of Bergell rocks from central Alps and Bergell boulders in Oligocene sediments. *Earth and Planetary Science Letters*, **45**, 355–360.

WAGNER, R. 2005. *Tertiary tectonics and magmatism along the TRANSALP-Profile between the Tauern Window and the Periadriatic Line (Eastern Alps)*. PhD thesis, Freie Universität Berlin, Germany.

WAWRZYNIEC, T. F., SELVERSTONE, J. & AXEN, G. J. 2001. Styles of footwall uplift along the Simplon and Brenner normal fault systems, Central and Eastern Alps. *Tectonics*, **20**, 748–770.

WEMMER, K. 1991. K/Ar-Altersdatierungsmöglichkeiten für retrograde Deformationsprozesse im spröden und duktilen Bereich – Beispiele aus der KTB Vorbohrung (Oberpfalz) und dem Bereich der Insubrischen Linie (N-Italien). *Göttinger Arbeiten der Geologie und Paläontologie*, **51**, 1–61.

WENK, H.-R. 1978. Are pseudotachylites the product of fracture or fusion? *Geology*, **6**, 507–511.

WIEDENBECK, M. 1986. Structural and isotopic age profile across the Insubric Line, Mello, Valtellina, N. Italy. *Schweizerische Mineralogische und Petrographische Mitteilungen*, **66**, 211–217.

WHEELER, J. & BUTLER, W. H. 1993. Evidence for extension in the western Alpine orogen: the contact between the oceanic Piemonte and overlying continental Sesia units. *Earth and Planetary Science Letters*, **117**, 457–474.

ZIMMERMANN, R., HAMMERSCHMIDT, K. & FRANZ, G. 1994. Eocene high-pressure metamorphism in the Pennine units of the Tauern window (Eastern Alps): Evidence from 40Ar–39Ar dating and petrological investigations. *Contributions to Mineralogy and Petrology*, **117**, 175–186.

ZINGG, A. & HUNZIKER, J. C. 1990. The age of movements along the Insubric Line West of Locarno (northern Italy and southern Switzerland). *Eclogae Geologicae Helvetiae*, **83** (3), 629–644.

ZINGG, A., HANDY, M. R., HUNZIKER, J. C. & SCHMID, S. M. 1990. Tectonometamorphic history of the Ivrea Zone and its relation to the crustal evolution of the Southern Alps. *Tectonophysics*, **182**, 169–192.